Pedosphere doi:10.1016/j.pedsph.2026.04.010
ISSN 1002-0160/CN 32-1315/P

Published by Elsevier B.V. and Science Press

Review Article

Geochemical transformation of ferrihydrite: A review on mechanisms, effects of coexisting molecules and environmental implications

Yupeng YAN[1], Cheng WANG[2], Muammar MANSOR[3], Rui JIANG[4], Xiaoming WANG[2], Qin ZHANG[1], Xionghan FENG[2], Wenfeng TAN[2], Andreas KAPPLER[3] and Biao WAN[2,*]

[1]*Key Laboratory of Poyang Lake Watershed Agricultural Resources and Ecology of Jiangxi Province, College of Land Resources and Environment, Jiangxi Agricultural University, Nanchang 330045 (China)*
[2]*Key Laboratory of Arable Land Conservation (Middle and Lower Reaches of Yangtze River), Ministry of Agriculture and Rural Affairs, College of Resources and Environment, Huazhong Agricultural University, Wuhan 430070 (China)*
[3]*Geomicrobiology, Department of Geosciences, University of Tuebingen, Tuebingen 72076 (Germany)*
[4]*Institute of Soil Science, Chinese Academy of Sciences, Nanjing 211135 (China)*

(Received August 7, 2025; revised January 24, 2026; accepted April 21, 2026)

ABSTRACT

Ferrihydrite is ubiquitous in soils and sediments. It can affect the speciation, transformation, and fate of nutrients, organic matter, and pollutants in these environments through adsorption, coprecipitation, and redox reactions. In oxic environments, ferrihydrite slowly transforms into more thermodynamically stable and crystalline iron minerals, regulated by a variety of environmental factors (*e.g.*, temperature, pH, and the presence of other substances). In anoxic environments (*e.g.*, waterlogged soils and wetland sediments), dissolved Fe(II) formed from Fe(III) reduction can remarkably accelerate ferrihydrite transformation into more crystalline iron(III)-bearing (oxyhydr)oxides (*e.g.*, goethite, lepidocrocite, and magnetite). Geochemical/abiotic ferrihydrite transformation affects its association with nutrients, organic matter, and pollutants. In reverse, the presence of anions/cations, organic matter, or ligands changes the rate and extent of Fe(II)-catalyzed ferrihydrite transformation, as well as the transformation pathways and the crystalline structures of Fe-bearing products. Fe(II)-induced ferrihydrite transformation is usually inhibited by the presence of surface-associated or coprecipitated substances. The associated trace anions/cations could be redistributed during Fe(II)-catalyzed ferrihydrite transformation into secondary iron oxide minerals. This review provides a comprehensive summary of abiotic ferrihydrite transformation with(out) dissolved Fe(II) and new perspectives on its environmental significance for the biogeochemical cycling of coexisting compounds.

Key Words: ferrihydrite, geochemical/abiotic transformation, anions/cations, organic matter, ligands, redistribution

*Corresponding author. E-mail: biao.wan@mail.hzau.edu.cn.

Citation: Yan Y P, Wang C, Mansor M, Jiang R, Wang X M, Zhang Q, Feng X H, Tan W F, Kappler A, Wan B. 2026. Geochemical transformation of ferrihydrite: A review on mechanisms, effects of coexisting molecules and environmental implications. *Pedosphere*. https://doi.org./10.1016/j.pedsph.2026.04.010.

INTRODUCTION

Iron(III) (oxyhydr)oxides (hereon denoted as Fe(III) oxides) are one of the most important and reactive groups of substances in soils, sediments, and aquatic environments (Cornell and Schwertmann, 2003; Huang *et al.*, 2021). Among different Fe(III) oxides, ferrihydrite is one of the most important, playing a key role in biogeochemical cycling, and is of particular interest to geochemists due to its poor crystallinity (short-range order), large specific surface area (> 300 m^2 g^{-1}), charged surface functional groups, and high abundance and reactivity (Wang *et al.*, 2013; Chappell *et al.*, 2017). Ferrihydrite is known to strongly associate with nutrients, metals, contaminants, and natural organic matter (NOM, a mixture of organic compounds resulting in nature from the degradation of biopolymers, *e.g.*, humic acid (HA) and fulvic acid (FA)) *via* surface adsorption and coprecipitation, thereby regulating their mobility, transformation and fate in natural environments (ThomasArrigo *et al.*, 2018; Sheng *et al.*, 2020a; Kappler *et al.*, 2021).

Generally, nano-sized ferrihydrite is the first solid to be precipitated upon Fe(III) hydrolysis. However, it is thermodynamically unstable in comparison to crystalline Fe(III) oxides, such as goethite (α-FeOOH), lepidocrocite (γ-FeOOH), hematite (α-Fe_2O_3), and magnetite (Fe_3O_4) (Navrotsky *et al.*, 2008; Boland *et al.*, 2014b). Ferrihydrite is always considered to be the precursor of crystalline Fe(III) oxide phases (Cornell and Schwertmann, 2003). Ferrihydrite tends to slowly transform into more thermodynamically stable Fe(III) minerals under low-temperature environmental conditions (Qafoku *et al.*, 2020; Sheng *et al.*, 2020a). The transformation kinetics and the formed products are strongly controlled by different environmental factors, including solution pH, temperature, redox potential, and the presence of organic or inorganic compounds (Qafoku *et al.*, 2020).

At ambient temperature and circumneutral pH, ferrihydrite transformation is kinetically slow, taking months to years under oxic conditions (Qafoku *et al.*, 2020; Sassi and Rosso, 2022). The extremely low solubility of surface Fe(III) restricts aqueous mass transfer and dissolution-reprecipitation at circumneutral pH (Qafoku *et al.*, 2020). In contrast, in anoxic environments (*e.g.*, flooded paddy soils, poorly drained soils and sediments, shallow aquifers, groundwaters, and monimolimnion of lakes), geochemically or microbially derived ferrous iron (Fe(II)) could induce ferrihydrite transformation into new Fe minerals (Grigg *et al.*, 2022; Lv *et al.*, 2022; Schulz *et al.*, 2023). Laboratory (abiotic) model studies have unequivocally demonstrated that Fe(II) catalyzed the transformation of ferrihydrite into crystalline Fe(III) oxides, such as lepidocrocite, goethite, and magnetite (Boland *et al.*, 2014b; Furcas *et al.*, 2023; Cheng *et al.*, 2025). It is thus important to note, however, that the specific mineral products formed in complex natural matrices like soils may differ from those in laboratory-controlled systems (Grigg *et al.*, 2022; Notini *et al.*, 2023; Schulz *et al.*, 2024).

Additionally, Fe(II)-catalyzed ferrihydrite transformations or recrystallization have wide implications, as the differences in properties of various Fe(III) oxides, such as surface area, reactivity and solubility, can influence the mobility (solid-solution distribution) and environmental fate of contaminants, nutrients, and organic matter (OM) that were initially adsorbed on or coprecipitated with ferrihydrite (Boland *et al.*, 2014b; Chen *et al.*, 2015). While the biogeochemistry of iron oxides has been extensively reviewed (Huang *et al.*, 2021; Liu *et al.*, 2022a; Lv *et al.*, 2022), a systematic synthesis focusing on the abiotic transformation mechanisms of ferrihydrite and their direct control over the fate of co-present substances is still lacking. This review mainly addresses two key questions: i) How do common environmental constituents (*e.g.*, anions, cations, and dissolved organic matter (DOM)) mechanistically alter the pathways and products of ferrihydrite transformation in the absence or presence of aqueous Fe(II)? ii) How do these transformation pathways, in turn, dictate the sequestration or release of associated nutrients and pollutants? We adopt a deliberately abiotic focus on isolating and clarifying the fundamental geochemical principles-such as interfacial electron transfer, nucleation constraints, and competitive sorption-that underpin ferrihydrite reactivity and transformation fate. It is precisely because microbial Fe(III) reduction in natural environments can exert complex effects on Fe

mineral transformation that establishing this abiotic "baseline" is critical. Our review could thus provide the mechanistic framework necessary to disentangle biologically mediated factors from purely geochemical drivers in the complex environments. By systematically summarizing recent literature, this review builds a predictive mechanistic link between specific chemical conditions, transformation trajectories, and potential environmental influences. We aim to offer a refined toolkit for interpreting ferrihydrite transformation dynamics and their profound impact on nutrient availability, contaminant fate, and carbon cycling in various environments.

STRUCTURAL CHARACTERISTICS OF FERRIHYDRITE

The basic structure, composition, and structural disorder of ferrihydrite are essential knowledge for geochemists to understand its reactivity, stability, and magnetic behavior, as well as the alterations of these properties during aging and transformation (Michel *et al.*, 2010). On the basis of structural analysis using the pair distribution function (PDF) method, the chemical formula of ferrihydrite was first reported as $Fe_{10}O_{14}(OH)_2$ (Michel *et al.*, 2007). Then, in 2010, Michel *et al.* further proposed a new model about the composition of ordered and disordered ferrihydrite, which was $Fe_{10}O_{14}(OH)_2$+~H_2O and $Fe_{8.2}O_{8.5}(OH)_{7.4}$+3$H_2O$, respectively, by combining detailed structural information with measured total Fe and hydration losses from thermogravimetric analyses (Michel *et al.*, 2010). The typical crystallite size of ferrihydrites is between 1 and 10 nm (Michel *et al.*, 2007; Wang *et al.*, 2013, 2016). Ferrihydrite is generally designated as two-line ferrihydrite (2LFh) or six-line ferrihydrite (6LFh) based on the number of poorly defined, broadened Bragg peaks in its X-ray diffraction (XRD) pattern (Michel *et al.*, 2007; Wang *et al.*, 2016). Poorly crystalline 2-line ferrihydrite has two broad reflections with d-spacing (or 2θ) values of 2.50 Å (35.8°) and 1.51 Å (62.7°). In contrast, 6-line ferrihydrite showed six reflections (peaks or lines) at d-spacing values (or 2θ) of 2.50 Å (35.8°), 2.21 Å (40.7°), 1.96 Å (46.3°), 1.72 Å (53.2°), 1.51 Å (61.9°) and 1.48 Å (63.4°) (Janney *et al.*, 2000; Wang *et al.*, 2013, 2016). Ferrihydrites with crystallinity between 2LFh and 6LFh have been reported, such as three-line ferrihydrite (3LFh), four-line ferrihydrite (4LFh), and five-line ferrihydrite (5LFh) (Wang *et al.*, 2013, 2016), which present different reflections in the XRD patterns. In addition, some synthetic silicon-containing (siliceous) ferrihydrite has been shown to have seven lines with comparatively sharp reflections (Schwertmann *et al.*, 2004; Berquó *et al.*, 2007).

Ferrihydrite has a hexagonal close-packed anion lattice, consisting of a mixture of defective and defect-free structural units, with variable hydroxyl and water adsorption or incorporation (Sassi *et al.*, 2021). In simulated single-crystal electron-diffraction patterns, two-line ferrihydrite contains highly disordered materials and nanocrystals with structures using hexagonal (ABAB) and cubic (ABC) stacking of close-packed layers of O^{2-} and OH^- ions. The structure of cubic stacking is similar to maghemite and has ~25% of Fe atoms in tetrahedral sites; the structure of hexagonal stacking consists of double chains of face-sharing Fe octahedra (Janney *et al.*, 2000).

Determining the definitive atomic structure of nano-sized ferrihydrite has been a long-standing challenge. To reveal ferrihydrite structural characteristics, a variety of spectroscopic techniques has been applied, including Mössbauer spectroscopy (MS), electron energy loss spectroscopy (EELS), X-ray absorption near edge structure spectroscopy (XANES), extended X-ray absorption fine structure spectroscopy (EXAFS), and PDF analysis of X-ray and neutron total scattering spectroscopy (Michel *et al.*, 2007; Harrington *et al.*, 2011; Peak and Regier, 2012). Several competing structural models have been proposed over time, including a single-phase model (Michel *et al.*, 2007, 2010; Pinney *et al.*, 2009; Chappell *et al.*, 2017), multi-phase or multi-domain models (Drits *et al.*, 1993; Manceau, 2009; Marchand and Rancourt, 2009; Funnell *et al.*, 2020), and a hybrid model (Gilbert *et al.*, 2013).

The scientific debate was crystallized in the late 2000s with the proposal of two fundamentally different single-phase models. The Michel model, derived from PDF analysis, proposed a structure (hexagonal space group P63mc) containing 20%--30% tetrahedrally coordinated Fe(III), with a core motif related to a Fe_{13} Keggin cluster (Michel *et al.*, 2007; Maillot *et al.*, 2011). This model was supported by subsequent Fe L-edge X-ray absorption spectroscopy (Peak and Regier, 2012) and PDF analysis of neutron total scattering spectroscopy (Harrington *et al.*, 2011). In contrast, the Manceau model posited a structure composed entirely of octahedral Fe, described as a "modified akdalaite" (Manceau *et al.*, 2014). Ab initio thermodynamic calculations based on density functional theory later suggested that nanoparticles based on either model could be thermodynamically stable under varying

temperature and water pressure conditions, potentially explaining the divergence (Sassi *et al.*, 2021).

An earlier and alternative viewpoint is represented by multi-phase models, such as the Drits model, which describes ferrihydrite as a nanocomposite of a defect-free phase (f-phase, $FeO_{0.85}OH$) and a defective phase (d-phase, FeOOH), possibly with traces of ultra-disperse hematite or maghemite (Drits *et al.*, 1993; Manceau, 2009). Attempts to reconcile these views have led to a hybrid model in which a combination of structural motifs from different models provides the best fit to experimental data (Gilbert *et al.*, 2013).

Despite extensive research, a definitive atomic-scale model for ferrihydrite remains elusive due to its inherent nanoscale disorder. A key emerging consensus is that its nanoparticles likely exhibit a core-shell architecture, featuring a relatively ordered core and a defective, hydration-rich surface that governs its high reactivity (Hiemstra, 2013; Weatherill *et al.*, 2016). However, several fundamental controversies persist, primarily revolving around three interconnected questions: (i) the validity and extent of tetrahedral Fe(III) incorporation, as proposed in the Michel model; (ii) whether the structure is best described as a single phase or a composite of distinct domains; and (iii) how the precise atomic arrangement at the surface differs from the core and controls interfacial processes. Consequently, ferrihydrite is more accurately viewed as a dynamic nanostructure whose specific atomic configuration is sensitive to synthesis conditions and environment. This fundamental structural ambiguity directly influences the interpretation of the mineral's stability, transformation pathways, and role in biogeochemical cycles.

TRANSFORMATION OF FERRIHYDRITE IN FE(II)-FREE SYSTEMS

Ferrihydrite is thermodynamically unstable with respect to highly crystalline iron oxides such as lepidocrocite, goethite, magnetite, and hematite (Navrotsky *et al.*, 2008), as shown in Fig. 1A. Ferrihydrite serves as the most important precursor for the formation of other crystalline Fe(III) oxides (*i.e.*, hematite and goethite) produced in the natural environment during weathering or pedogenic processes (Cornell & Schwertmann, 2003; Wang *et al.*, 2016). Its transformation results in a decrease in surface area and a subsequent decrease in the ability to sequester contaminants (Das *et al.*, 2011b).

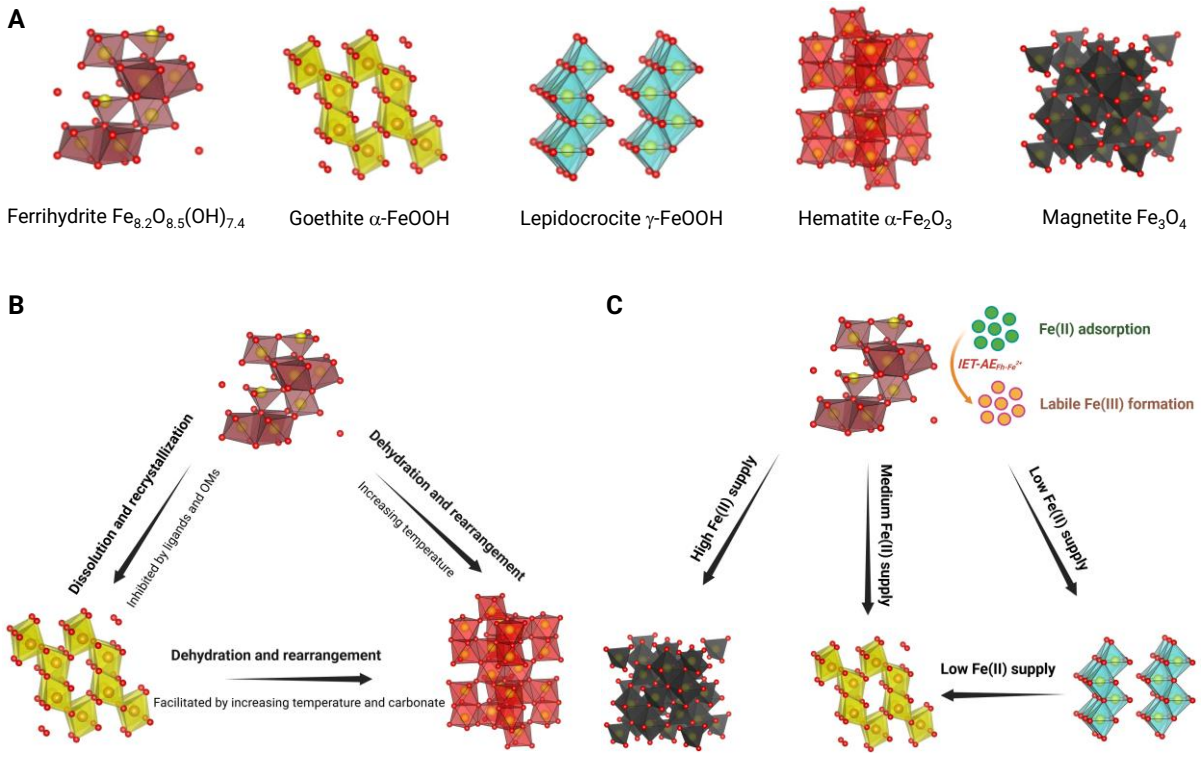

Fig. 1 (A) Schematic diagrams of ferrihydrite, goethite, lepidocrocite, hematite, and magnetite crystal structures,

respectively. The red and yellow dots are oxygen and iron atoms, respectively. (B) Transformation processes of ferrihydrite under Fe(II)-free conditions (Das *et al.*, 2011b; Soltis *et al.*, 2016; Li *et al.*, 2020, 2022). (C) Fe(II)-catalyzed transformation processes of ferrihydrite. Both Fe(II) surface-complexed concentration and Fe(II) transfer rate to ferrihydrite structure affect the identity and formation rate of secondary minerals, and labile Fe(III) plays a key role in Fe(II)-catalyzed ferrihydrite transformation (Boland *et al.*, 2014b; Qafoku *et al.*, 2020; Liu *et al.*, 2022b, 2023). IET-$AE_{Fh-Fe^{2+}}$ means interfacial electron transfer and atom exchange of ferrihydrite with Fe(II).

Transformation mechanism

Two-line ferrihydrite transforms to goethite or hematite either through a dissolution–recrystallization (dissolution and reprecipitation) process (with goethite being intermediary) with the mass fraction of the more stable phase increasing at the expense of the dissolving phase (Das *et al.*, 2011b; Soltis *et al.*, 2016), or through a solid state-phase transformation (solid-state recrystallization or topotactic transformation) (Cudennec *et al.*, 2006; Das *et al.*, 2011b; Soltis *et al.*, 2016), as shown in Fig. 1B. Cryogenic transmission electron microscopy, XRD, and low temperature magnetometry demonstrated that the formation of hematite from the aggregation of ferrihydrite particles followed a solid-state phase transformation, consistent with a particle-mediated growth mechanism, possibly *via* oriented attachment (Soltis *et al.*, 2016).

Factors influencing ferrihydrite transformation

The transformation of ferrihydrite to crystalline Fe minerals is usually dependent on reaction pH, transformation temperature, water chemistry conditions (*e.g.*, coexisting or coprecipitated ions/ligands/DOM), particle size, transformation time, as well as the preparation procedures of ferrihydrite (Cudennec *et al.*, 2006; Liu *et al.*, 2010a; Das *et al.*, 2011b; Namayandeh *et al.*, 2022).

Temperature and pH. The rate of ferrihydrite transformation in the absence of coexisting substances increases with increasing pH and temperature (Li *et al.*, 2020). Generally, high temperature favors the formation of hematite (Cudennec *et al.*, 2006). The rate of ferrihydrite transformation increases by about 5 orders of magnitude from 25 to 100 °C at pH 10 (Das *et al.*, 2011b).

However, pH is a more complicated factor that regulates ferrihydrite transformation, necessitating the consideration of other factors at the same time. Low and high values of pH (2–5 and 10–14) favor the formation of goethite *via* dissolution and recrystallization (reprecipitation), while hematite formation is favored at neutral pH (values around 7) *via* dehydration and internal atomic arrangement at room temperature (Schwertmann and Murad, 1983; Schwertmann *et al.*, 2004; Cudennec *et al.*, 2006; Li *et al.*, 2020). It was also reported that at higher temperatures (50−100 °C), hematite was the dominant product in the pH range of 2 to 10 because a two-stage crystallization process was observed, with goethite being an intermediary (Das *et al.*, 2011b). High temperature and neutral pH favor ferrihydrite transformation into hematite by dehydration-aggregation, while high or low pH promotes the formation of goethite through dissolution-recrystallization in aqueous systems (Das *et al.*, 2011b).

The calculated first-order rate constants (k) of ferrihydrite transformation increased exponentially with respect to the pH and followed the progression $\log_{10} k = \log_{10} k_0 + a \cdot pH^3$ ($k_0 = 1.01 \times 10^{-4}$ h^{-1}) (Furcas *et al.*, 2023). Simultaneous monitoring of the concentration of aqueous Fe(III) demonstrated that goethite likely precipitated from solution, and its formation was rate-limited by the comparatively slow redissolution of ferrihydrite (Furcas *et al.*, 2023).

Solution composition. The transformation products of ferrihydrite are also dependent on the solution composition (*e.g.*, background electrolyte). In the presence of nitrate, the transformation products included hematite (major) and goethite (minor) under acidic conditions (pH 4) and only hematite under alkaline conditions (pH 8) (Zhang *et al.*, 2018). By contrast, in the presence of sulfate, goethite was the dominant product under slightly acidic conditions (pH 4) with 6-line ferrihydrite as the intermediate product, whereas under slightly alkaline conditions, the formation of hematite was favored (Zhang *et al.*, 2018).

Metal cations. Coprecipitated or sorbed metal cations may either inhibit or promote ferrihydrite transformation in Fe(II)-free systems (Ye *et al.*, 2021; Ding *et al.*, 2022b; Zhang *et al.*, 2022). For example, coprecipitated or structurally incorporated Al(III) hindered the transformation of ferrihydrite

and changed the aging products by inhibiting the dissolution of ferrihydrite (Ye *et al.*, 2021; Zhang *et al.*, 2022). An increase in Zn(II) retarded the transformation rate of ferrihydrite drastically. At and below 200 μmol L^{-1} Zn(II), most of the ferrihydrite was transformed directly to hematite and goethite, while at 750 μmol L^{-1} Zn(II), ferrihydrite was transformed to hematite with Zn-bearing maghemite (Fe_2O_3 or $Fe_{2.67}O_4$) being an intermediate, metastable phase (Sakakibara *et al.*, 2019). Rare earth elements (REEs) inhibit ferrihydrite transformation into goethite and hematite at pH 5 and 7, respectively, by suppressing dissolution and recrystallization at pH 5 and primarily through structural incorporation at pH 7 (Yang *et al.*, 2021).

Anions, oxyanions, organic ligands, and organic matter. Generally, coexisting, adsorbed, or coprecipitated substances (*e.g.*, anions, oxyanions, organic ligands, and OM) can inhibit or enhance ferrihydrite transformation in Fe(II)-free systems and affect the morphology of products based on their types and structures. Anions and oxyanions retard the thermal dissolution and transformation of ferrihydrite (Ford, 2002; Das *et al.*, 2011a). For instance, the extent of ferrihydrite transformation into hematite decreased with increasing As/Fe ratios but increased at a higher heating temperature (Wang *et al.*, 2015). The transformation of ferrihydrite coprecipitated with arsenate was significantly retarded at or above an arsenate solid loading of 29.5 g As kg^{-1} ferrihydrite (As/Fe = 0.042) (Ford, 2002).

Recently, it was reported that the type and strength of surface oxyanion complexes govern the kinetics and pathway of ferrihydrite transformation (Namayandeh *et al.*, 2022). Kinetic modeling showed a significant decrease in the rate of ferrihydrite transformation for oxyanion surface complexes dominated by strong inner-sphere (*e.g.*, PO_4^{3-}, AsO_4^{3-}, and SO_4^{2-}) versus weak outer-sphere (*e.g.*, NO_3^-) complexation and the control (Namayandeh *et al.*, 2022, 2023). Oxyanions (*e.g.*, AsO_4^{3-} and PO_4^{3-}) dehydrated the surface of ferrihydrite through inner-sphere complexes, which delayed the dissolution-recrystallization pathway and promoted aggregation, resulting in increased hematite formation (Namayandeh *et al.*, 2023, 2024).

However, under certain conditions, enhanced transformation was also observed. The presence of antimonate (SbO_4^{3-}, Sb(V)) enhanced the transformation of Al-coprecipitated ferrihydrite (Ye *et al.*, 2021). It was proposed that the presence of Sb(V) weakened the inhibition of Al(III) under experimental conditions. Competitive reaction of Al(III) and Sb(V) for substitution on the lattice Fe of ferrihydrite likely decreased Al(III) substitution on ferrihydrite and thus increased the observed transformation rate of ferrihydrite (Ye *et al.*, 2021). In addition, (bi)carbonate can change ferrihydrite transformation pathways and facilitate the transformation of ferrihydrite to hematite, retarding goethite formation (Li *et al.*, 2020). Moreover, carbonate could override the retarding impact of phosphate on ferrihydrite transformation and promote the formation of more crystalline rhombic hematite particles *via* olation reaction (Li *et al.*, 2022).

Organic ligands or NOM with phosphate, carboxyl, or hydroxyl groups have strong adsorption affinity with ferrihydrite, thus inhibiting the transformation of ferrihydrite (Hu *et al.*, 2018; Zhang *et al*., 2024; Pan *et al.*, 2025). For example, the presence of organic ligands/OM can control the processes of dissolution-recrystallisation under acidic conditions (pH < 7) and/or solid-state aggregation under neutral conditions (pH ~7) (Zhao *et al.*, 2022c). Carboxyl and hydroxyl groups in microplastic-derived DOM were found to increase Fe–O bond length by 0.02–0.03 Å through interacting with Fe atoms in the first shell, then inhibiting the transformation of ferrihydrite to hematite (Zhang *et al*., 2024). Several mechanisms are proposed to explain the inhibitive effects of organic ligands and OM: (i) organic ligands/OM block surface sites and retard the hydrolysis and dissolution of surface Fe dimers and/or polymers, which then inhibits the rearrangement or crystallization process of ferrihydrite into more crystalline phases and the later growth (Chen *et al.*, 2020); (ii) the interaction of ferrihydrite with organic ligands/OM results in a significant increase of the surface negative charges, which reduces its aggregation, precluding the dehydration and rearrangement processes to form hematite (Sun *et al.*, 2021); and (iii) organic ligands/OM could complex with aqueous Fe(III) to inhibit its nucleation (Zhao *et al.*, 2022c).

Other factors. Particle size, water content, and coexisting solid natural substances could also affect ferrihydrite transformation under Fe(II)-free conditions. Their specific effects are outlined as follows. First, poorly crystalline ferrihydrite is metastable with respect to the formation of both hematite and goethite at 298.15 K, but may be stabilized at small particle sizes due to its favorably low surface formation energy (Pinney *et al.*, 2009). When the sizes are larger than 8 nm, the thermodynamic stability of ferrihydrite sharply drops with increasing particle size, leading to the formation of nano-goethite and

nano-hematite during its aging (Hiemstra, 2015). Second, water proves to be critical for the nucleation of hematite domains in ferrihydrite, the resulting crystallite orientation, and the underlying crystallization mechanism (Arinchtein *et al*., 2020). Water holding capacity or water content is expected to be a direct factor controlling ferrihydrite transformation and dissolution processes in soils (Zhang *et al*., 2018). Moreover, coexisting solid natural substances (*e.g.*, clay minerals and substrate hematite) could decline the aggregation of ferrihydrite (Yan *et al*., 2021; Zhang *et al*., 2023) or modulate the dissolution-recrystallization process (Wei *et al*., 2025), thus affecting its phase transformation.

KINETICS AND THERMODYNAMIC MECHANISMS OF FE(II)-CATALYZED FERRIHYDRITE TRANSFORMATION

Under anaerobic conditions, the presence of aqueous Fe(II) could accelerate the transformation of ferrihydrite. The process of Fe(II)-catalyzed transformation of ferrihydrite has been extensively studied as it is considered to be the main pathway for the evolution of iron oxide minerals in natural environments. The transformation usually yields goethite, lepidocrocite, or/and magnetite (Fig. 1C), the presence and proportions of which depend on reaction conditions (*e.g.*, pH, temperature, the Fe(II) and ferrihydrite concentration, the Fe(II)/Fe(III) ratio, the solid to solution ratio, background ligand, buffer selected, and pore space size) as we discussed in the previous section (Hansel *et al.*, 2005; Boland *et al.*, 2014b; ThomasArrigo *et al.*, 2018; Hua *et al.*, 2023). Advanced characterization techniques, such as X-ray absorption spectroscopy (XAS), ^{57}Fe MS, bulk XRD, micro XRD (μXRD), transmission electron microscopy, and Fourier transform infrared spectroscopy (FTIR) could be used to monitor this process (ThomasArrigo *et al.*, 2017; Xiao *et al.*, 2017; Sheng *et al.*, 2020b; Notini *et al.*, 2022) and to reveal its reaction mechanism in reducing environments.

Effect of temperature and pH

In the presence of Fe(II), the transformation of poorly ordered ferrihydrite into crystalline minerals is rapid and highly dependent on temperature and pH (Hansel *et al.*, 2005; Liu *et al.*, 2007; Boland *et al.*, 2014b). The time-resolved peak area data fitted using the kinetic model yielded rate constants of 4.0×10^{-5}, 1.3×10^{-4}, 3.3×10^{-4}, 2.27×10^{-3}, and 3.14×10^{-3} s^{-1} at reaction temperatures of 21, 45, 60, 85, and 90 °C, respectively (Yee *et al.*, 2006). The activation energy for Fe(II)-catalyzed transformation of ferrihydrite was determined to be 56 ± 4 kJ mol^{-1} (Yee *et al.*, 2006). Comparison with the activation energy predicted for the phase conversion in the absence of Fe(II) indicated that Fe(II) acted as a catalyst that decreased the activation energy barrier by 38 kJ mol^{-1} (Yee *et al.*, 2006).

It was reported that Fe(II) works as a catalyst to promote ferrihydrite transformation *via* two mechanisms: catalytic dissolution-reprecipitation and catalytic solid-state transformation (Liu *et al.*, 2005, 2007). High temperatures with high pH values (from 5 to 9) were more favorable to solid-state transformation, leading to the formation of hematite. Low temperatures and low pH values were more supportive for dissolution–reprecipitation mechanism, resulting in the formation of lepidocrocite or goethite, which depends on aqueous Fe(II) concentrations (Liu *et al.*, 2007). The lepidocrocite phase was generally more prevalent at relatively low pH and low total [Fe(II)] conditions, while higher pH and more total [Fe(II)] generally resulted in faster production of goethite (Boland *et al.*, 2014b). Higher pH values result in both higher solid-associated Fe(II) concentrations and higher precipitation of ferrous hydroxides during Fe(II)-catalyzed recrystallization. The rate of goethite production increased with both an increase in solid-associated Fe(II) concentrations (at higher pH) and rate of Fe(II) transport from solution to solid (with increased rate driven particularly by higher aqueous Fe(II) supply (Boland *et al.*, 2014b).

Effect of Fe(II) concentration

The rate of ferrihydrite transformation and the nature of the products formed depend on Fe(II) speciation and concentration, and its sorption rate (Boland *et al.*, 2013, 2014b; Jones *et al.*, 2017; Qafoku *et al.*, 2020). Generally, at low Fe(II) levels (below 1 mmol L^{-1}), ferrihydrite converted to lepidocrocite and goethite *via* dissolution and reprecipitation. However, at higher Fe(II) levels (at and above 1.8 mmol L^{-1} Fe(II)), formation of magnetite was favored (Hansel *et al.*, 2005; Yang *et al.*, 2010;

ThomasArrigo *et al.*, 2017, 2018).

It is likely that, besides aqueous Fe(II) in solution, adsorbed Fe(II) and labile Fe(III) also play a key role in Fe(II)-catalyzed transformation of ferrihydrite. Quick-scanning XAS analysis revealed that the higher Fe(II) concentration resulted in a five-fold higher first-order rate constant for the conversion of ferrihydrite to goethite than at the lower Fe(II) concentration, despite surface complexation modelling indicating that similar concentrations of surface-adsorbed Fe(II) species were present under both conditions. It was suggested that bulk solution Fe(II) concentrations rather than surface-adsorbed Fe(II) concentrations controlled the crystallization kinetics of ferrihydrite to goethite (Boland *et al.*, 2013).

It was further reported that adsorbed Fe(II) is a more facile reductant than aqueous Fe(II) (Jones *et al.*, 2017). The concentration of solid-associated Fe(II) and the rate of transport of Fe(II) to Fe(III) oxide surface appeared to determine the formation phases and rates of secondary iron oxide minerals (Fig. 1C). Lepidocrocite growth was enhanced at lower solid-associated Fe(II) concentrations while conditions leading to more rapid sorption of Fe(II) from solution led to higher goethite growth rates (Boland *et al.*, 2014b).

Meanwhile, labile Fe(III) species could play a key role in ferrihydrite transformation and recrystallization of newly formed Fe(III) oxides (Amstaetter *et al.*, 2010; Sheng *et al.*, 2020b; Latta *et al.*, 2023). Labile Fe(III) is an active Fe(III) intermediate species resulting from oxidation of Fe(II) sorbed on ferrihydrite surface, followed by interfacial electron transfer and atom exchange of ferrihydrite with Fe(II) (Sheng *et al.*, 2020a, b). Labile Fe(III) intermediate species could be measured using the Fe(III)-specific complexing agent xylenol orange (Sheng *et al.*, 2020a, b, 2021). ^{57}Fe isotope tracer experiments indicated that Fe(II) sorption followed by interfacial Fe(II)-Fe(III) electron transfer generated this labile Fe(III) species, usually with a much higher aqueous solubility (Sheng *et al.*, 2020b). Oxidation of sorbed Fe(II) by ferrihydrite also yielded a labile Fe(III) product on the ferrihydrite surface that was chemically distinct and more labile than structural Fe(III) within ferrihydrite, as indicated by an isotope-labeling experiment (Sheng *et al.*, 2020b). Labile Fe(III) as the key "seed" species led to the nucleation and growth of more crystalline Fe(III) oxide phases during Fe(II)-catalyzed ferrihydrite transformation (Sheng *et al.*, 2020a, b). The transformation pathway as well as the promotive effect of Fe(II) could be explained on a unified basis of the kinetics of Fe(III) olation and oxolation reactions, which is necessary to nucleate and sustain the growth of lepidocrocite/goethite products, and the formation of crystalline iron oxides were greatly accelerated by labile Fe(III) (Fig. 1C) (Sheng *et al.*, 2020b). Another study then indicated that the supersaturation of labile Fe(III) intermediate, not the starting Fe(II)/ferrihydrite ratios, controlled the formation rates of the product mineral phases (Sheng *et al.*, 2021). Similar to ferrihydrite, the conversion of lepidocrocite to product phases (magnetite or goethite) occurred by a dissolution–reprecipitation mechanism mediated by $Fe(III)_{labile}$ (Liu *et al.*, 2022b). Recently, it was reported that the photoexcited triplet state of riboflavin could significantly accelerate interfacial electron transfer from Fe(II) to ferrihydrite, increasing the reductive dissolution rate of ferrihydrite and boosting the accumulation rate of the key intermediate labile Fe(III), and promoting the subsequent conversion of lepidocrocite to magnetite (Ding *et al.*, 2024).

Effect of ferrihydrite particle size and crystallinity

Particle size and crystallinity affect the mineral transformations of ferrihydrite and iron oxides in the presence of Fe(II). It was found that ferrihydrite and 5-nm-sized lepidocrocite crystals attained complete isotopic equilibration with aqueous Fe(II) within < 3 d. Within this timeframe, ferrihydrite completely transformed into new and more stable phases such as lepidocrocite and goethite. Lepidocrocite and goethite, having larger particles (20 nm-sized), required a longer time (> 7 d) to reach isotopic equilibrium (Pedersen *et al.*, 2005).

Ferrihydrite with low crystallinity had a relatively high redox potential, corresponding to the faster Fe(II)-ferrihydrite interfacial electron transfer and Fe(III) labile production. With the increase of initial Fe(II) concentration from 0.2 to 5.0 mmol L^{-1}, the transformation pathways of ferrihydrite with varying degrees of crystallinity changed (Liu *et al.*, 2023).

Molecular mechanism of Fe(II)-catalyzed ferrihydrite transformation

Fe(II)-catalyzed transformation of ferrihydrite to new crystalline phases (*e.g.*, goethite and

lepidocrocite) involved several physicochemical processes: (i) adsorption of Fe(II) to the ferrihydrite surface, (ii) the immediate oxidation of surface-adsorbed Fe(II) to Fe(III), (iii) the transfer of electrons to structural Fe(III) at the ferrihydrite surface (interfacial electron transfer between the aqueous as well as sorbed Fe(II) and structural Fe(III) in ferrihydrite acting as a semiconductor), (iv) the release of structural Fe(III) as Fe(II) ("atom exchange") to solution (*i.e.*, reductive dissolution of the ferrihydrite mineral and release of $Fe(II)_{(aq)}$), (v) producing a labile Fe(III) species by the oxidation of aqueous Fe(II) on ferrihydrite surface, and (vi) hydrolysis of labile Fe(III) intermediate and the recrystallization of the Fe(III) oxide phases (*i.e.*, formation of more crystalline and thermodynamically stable new phases) (Handler *et al.*, 2009; ThomasArrigo *et al.*, 2017; Yan *et al.*, 2022). Recently, (semi) *in-situ* μXRD and transmission electron microscopy (TEM) were employed to reveal the nucleation pathways of iron oxide nanoparticles during Fe(II)-catalyzed transformation of ferrihydrite (Gomez *et al.*, 2020; Qafoku *et al.*, 2020). It was confirmed that dissolution-reprecipitation and solution-mediated Fe mass transfer are critical for rapid crystal growth of new Fe mineral phases (Gomez *et al.*, 2020; Qafoku *et al.*, 2020).

Beyond pure Fe(II) catalysis, sunlight and ligands can also significantly alter ferrihydrite transformation kinetics and pathways *via* ligand-to-metal charge transfer (LMCT) processes (Lv *et al.*, 2022; Wang *et al.*, 2025). Solar irradiation can enhance electron transfer between aqueous Fe(II) and ferrihydrite, accelerating its transformation to goethite and lepidocrocite (Shu *et al.*, 2019, 2022). More directly, under simulated solar irradiation, the oxalate-mediated LMCT process synchronously initiated Fe(II) production and proton consumption, the latter of which facilitated interfacial electron transfer and atom exchange (IET-AE) processes between ferrihydrite and newly formed Fe(II). Ferrihydrite was thus prone to transform into goethite due to sufficient Fe(II) from the LMCT process and enough affinity of Fe(II) with the mineral to trigger IET-AE at pH 5.0–8.0 (Wang *et al.*, 2025). Thus, LMCT likely acts as an indirect catalytic amplifier of the Fe(II)-catalyzed pathway by providing a renewable source of aqueous Fe(II) and modulating interfacial chemistry. Recognizing these coupled pathways is essential for accurately predicting ferrihydrite stability and the associated fate of coexisting elements in diverse environmental settings.

EFFECT OF CO-PRESENT MOLECULES ON FE(II)-CATALYZED FERRIHYDRITE TRANSFORMATION

In natural environments, cations, anions, and OM/ligands are abundant and may be sorbed on ferrihydrite or coprecipitated with ferrihydrite. These cations, anions, and OM/ligands can thus influence the surface properties of ferrihydrite and its Fe(II)-catalyzed transformation.

Effect of cations

Considering the complexity of natural environments, phase transformation of ferrihydrite induced by aqueous Fe(II) is a critical geochemical reaction, which is greatly affected by coexisting cations or trace metals (incorporated in the structure of ferrihydrite or sorbed on the surface of ferrihydrite), such as Ca^{2+}/Mg^{2+}, rare earth elements (REEs), Mn(II), Co(II), Ni(II), and Zn(II) (Liu *et al.*, 2016, 2017; Fei *et al.*, 2018; Dong *et al.*, 2024). Cations could retard or promote the rate of Fe(II)-catalyzed ferrihydrite transformation to different extents, change the composition of the transformation products, and modify the transformation pathways, depending on their binding affinities to ferrihydrite (Hu *et al.*, 2022; Yan *et al.*, 2022; Zhao *et al.*, 2022a).

Generally, adsorbed rare earth elements (Fei *et al.*, 2018; Hua *et al.*, 2019; Yang *et al.*, 2021) or divalent cations (Gomez *et al.*, 2013; Liu *et al.*, 2016) were shown to inhibit Fe(II)-catalyzed ferrihydrite transformations and alter the amounts of goethite, lepidocrocite, and magnetite that formed at ambient temperature. Several mechanisms may explain the inhibitive effect of cations on ferrihydrite transformation: (i) the formation of strong covalent bonds between added cations and ferrihydrite could decrease the adsorption surface sites for Fe(II), block the electron transfer between Fe(II) and structural Fe(III), and consequently inhibit ferrihydrite dissolution and transformation (Katz *et al.*, 2012; Hu *et al.*, 2022; Shen *et al.*, 2022); (ii) the presence of cations may occupy the dissolution sites (*e.g.*, kink, edge, or defect sites) on ferrihydrite, thus hindering its polymerization and transformation (Hu *et al.*, 2020, 2022); and (iii) before ferrihydrite transformation, inner-sphere bidentate adsorption of cations on Fe mineral surfaces can distort the structure of the Fe-binding environment and change surface

coagulation and polymerization, and the subsequent normal crystal nucleation and crystal growth of secondary Fe minerals are alleviated or restricted (Liu *et al.*, 2016; Shen *et al.*, 2022; Zhao *et al.*, 2022a).

Particularly, divalent metal cations (denoted as Me(II), including Mg(II), Ca(II), Ba(II), Mn(II), Co(II), Ni(II), and Zn(II)) with strong binding affinities decreased the bound-Fe(II) amount on ferrihydrite and reduced the redox potentials of the Fe(II)-catalyzed system, which inhibits transformation (Liu *et al.*, 2016). The binding affinities of Me(II) thus play a key role in determining the pathway of Fe(II)-catalyzed transformation. Ferrihydrite was first transformed to lepidocrocite and then to goethite and magnetite with Me(II) that had a lower binding affinity than Fe(II), whereas it was directly transformed to goethite and magnetite with Me(II) that had a higher binding affinity than Fe(II) (Liu *et al.*, 2016).

The inhibition effect of REEs on Fe(II)-catalyzed transformation of ferrihydrite is dependent on their types as well as adsorptive affinity. For example, it was showed that the heavy REEs (*e.g.*, Ho(III) and Lu(III)) were more efficiently adsorbed on ferrihydrite and stabilized by the transformation products compared with the light REEs (*e.g.*, La(III), Ce(III)) due to the higher adsorptive affinity and smaller atomic radius of heavy REEs (Fei *et al.*, 2018; Hua *et al.*, 2019). Both heavy and light REEs can inhibit Fe atom exchange between Fe(II) and ferrihydrite, and sequentially, Fe(II)-catalyzed phase transformation, because of the competitive adsorption with Fe(II) on ferrihydrite surface (Fei *et al.*, 2018; Hua *et al.*, 2019).

Regardless of the Fe(II) concentration, aluminum substituted into or adsorbed on ferrihydrite led to significant inhibition of the formation of secondary iron minerals, resulting in ferrihydrite preservation. This is mainly because Al is redox-inactive and thus retards electron transfer (Hansel *et al.*, 2011; Huang *et al.*, 2021). Structural Al decreased Fe(II) retention/incorporation on/into ferrihydrite and impeded Fe(II)-catalyzed transformation, requiring nearly three-orders of magnitude higher Fe(II) concentrations to induce transformation compared to pure ferrihydrite (Masue-Slowey *et al.*, 2011). Furthermore, the characteristics of secondary mineral formation upon Fe(II) reaction with ferrihydrite were not only a function of Al concentration but also related to the mode of Al incorporation (Hansel *et al.*, 2011).

It was also reported that some elements substituting in ferrihydrite could promote the formation of hematite at ambient temperature (Yan *et al.*, 2022). During the Fe(II)-induced transformations of ferrihydrite containing zinc in its structure at pH 7, low Fe(II) concentration (0.2 mM) led to the formation of hematite plus minor lepidocrocite, whereas high Fe(II) concentration (1 mM) produced a magnetite-lepidocrocite mixture (Yan *et al.*, 2022).

Effect of anions

Anions (such as Cl^-, SO_4^{2-}, HCO_3^-, CO_3^{2-}, PO_4^{3-}, and SiO_3^{2-}) are ubiquitous in natural environments. The presence of these natural anions could affect the rates, extents, and pathways of Fe(II)-catalyzed ferrihydrite transformation and determine the phase/type, size, amount/quantity, and morphology of newly formed iron oxide minerals. Different anions showed different influence ability due to the varied affinity of these anions to the ferrihydrite surface (Hansel *et al.*, 2005; Liu *et al.*, 2008, 2010b; Qafoku *et al.*, 2020; Dong *et al.*, 2024; Ding *et al.*, 2025; Zhao *et al.*, 2025). Generally, coexisting anions inhibited the transformation of ferrihydrite to crystalline minerals by reducing the extent of electron transfer between Fe(II) and Fe(III) and hindering the dissolution, polymerization, and recrystallization of Fe(III).

Effects of bicarbonate, sulfate, and chloride. Fe(II)-catalyzed transformation of ferrihydrite in sulfate-rich medium differed from that in chloride (Cl^-) medium in the phase, the amount, and the morphology of products and transformation rate (Liu *et al.*, 2008). The rate and extent of ferrihydrite transformation were largely consistent with their affinity for iron oxides in the order bicarbonate (HCO_3^-) > sulfate (SO_4^{2-}) > Cl^- (Qafoku *et al.*, 2020). Cl^- medium favored the formation of lepidocrocite, while SO_4^{2-} medium supported the formation of both goethite and lepidocrocite at room temperature (Hansel *et al.*, 2005; Liu *et al.*, 2008; Qafoku *et al.*, 2020). Goethite particles obtained in Cl^- medium were star-like but rod-like in SO_4^{2-} medium. The transformation rate in the SO_4^{2-} medium was obviously slower than that in the Cl^- medium. The formation extent of lepidocrocite depended on both the ionic strength of the suspensions and the dissolution rate of ferrihydrite (Liu *et al.*, 2008).

Effect of silicate. Adsorbed or coprecipitated (structural impurity) silicate (Si) on/in

ferrihydrite could significantly change the reactivity of ferrihydrite and its transformation rate/newly formed products (Boland *et al.*, 2011; Schulz *et al.*, 2022). First, the adsorption of Si on ferrihydrite inhibited direct complexation of Fe(II) onto the mineral surface and reduced the likelihood of isotope/electron exchange between aqueous Fe(II) and ferrihydrite, thereby preventing Fe(II)-catalyzed ferrihydrite transformation (Jones *et al.*, 2009). Second, upon surface dissolution of Fe(III) minerals for electron exchange with aqueous Fe(II), Si prevented the recrystallisation to form more stable Fe(III) minerals, due to its tendency to inhibit the polymerization of its thermodynamically stable precursors (Jones *et al.*, 2009; Schulz *et al.*, 2022). For example, during Fe(II)-catalyzed transformations of ferrihydrite and Si-ferrihydrite, ferrihydrite transformed monotonically to goethite, whereas Si-ferrihydrite transformed into a form similar to ferrihydrite synthesized in the absence of silicate (Boland *et al.*, 2011).

Effect of phosphate. Phosphate exerts a multi-faceted influence on Fe(II)-catalyzed ferrihydrite transformation (Schulz *et al.*, 2024; Zhao *et al.*, 2025), since its impact is concentration-dependent and mediated by its association (*e.g.*, adsorbed on ferrihydrite or coprecipitated with ferrihydrite) (Zhao *et al.*, 2025). For adsorbed phosphate, as the P/Fe ratio increased from 0 to 0.01, the transformed mineralogy shifted from goethite towards mixtures containing magnetite and lepidocrocite, and ultimately to lepidocrocite being the dominant product. Phosphate modified the transformation pathways *via* promoting Fe(II) sorption, suppressing labile Fe(III) generation, and retarding Fe(III) oxides crystallization. At higher loadings (*e.g.*, P/Fe = 0.05), phosphate acted as a strong inhibitor of ferrihydrite transformation. Crucially, coprecipitated phosphate exerted a more potent inhibitory effect than adsorbed phosphate on ferrihydrite (Zhao *et al.*, 2025).

Effect of arsenate. The concentration and speciation of arsenate (As) are key factors affecting Fe(II)-induced transformation rates and pathways of ferrihydrite, as well as the mineralogy and morphology of the produced crystalline Fe(III) oxides. While low concentrations of adsorbed or coprecipitated As (As:Fe mol ratio <0.030) had a limited impact on ferrihydrite recrystallization and transformation rates, high concentrations of As (As:Fe molar ratio ≥ 0.224) can significantly inhibit ferrihydrite transformation into lepidocrocite (Pedersen *et al.*, 2006; Gomez *et al.*, 2013; Zhang *et al.*, 2019a). Different mechanisms were proposed to explain the effect of As(V) on the transformation of ferrihydrite: (i) As(V) formed covalent bonds on the surfaces of ferrihydrite, occupying adsorption sites and reducing the extent of electron transfer between Fe(II) and Fe(III); (ii) the presence of As(V) inhibited Fe-O-Fe polymerization by inducing distortions in the Fe bonding environment and inhibiting the crystal nucleation and growth; and (iii) the presence of As(V) blocked dissolution sites of ferrihydrite and then further impeded the polymerization of ferrihydrite to more thermodynamically stable iron oxides (Gomez *et al.*, 2013; Hu *et al.*, 2020).

Effect of selenite, hexahydroxyantimonate, and molybdate. Meanwhile, other coexisting anions, such as selenite (SeO_3^{2-}, Se(IV)), hexahydroxyantimonate ($[Sb(OH)_6]^-$, Sb(V)), and molybdate (MoO_4^{2-}, Mo(VI)), significantly modulate Fe(II)-catalyzed ferrihydrite transformation pathways and product assemblages by competing for adsorption site on Fe(III) oxide surfaces and altering local chemical conditions. Adsorbed Se(IV) inhibited Fe(II)-catalyzed recrystallization of ferrihydrite into goethite by inhibiting Fe atom exchange through competitive adsorption of Se(IV) with Fe(II) on Fe(III) oxides. Transmission electron microscopy images showed that pH values and the presence of Se(IV) had significant impacts on the morphology of the formed goethite (Wang *et al.*, 2020).

At low and medium Sb(V) loadings (Sb:Fe(III) molar ratios of 0.003 and 0.016), Fe(II) induced rapid transformation of ferrihydrite to goethite, with some lepidocrocite forming as an intermediate phase. In contrast, the highest Sb:Fe(III) molar ratio (0.08) inhibited lepidocrocite formation, decreased the extent of goethite formation, and instead resulted in the substantial formation of feroxyhyte at pH 7 (Hockmann *et al.*, 2021).

In the presence of 0.5 and 10.0 mmol L^{-1} $Fe(II)_{(aq)}$, MoO_4^{2-}-adsorbed ferrihydrite was transformed to lepidocrocite and goethite at pH 8, while 0.5 mmol L^{-1} $Fe(II)_{(aq)}$-induced phase transformation was inhibited for ferrihydrite-Mo containing both high (12.5) and low (31.5) Fe/Mo ratios at pH 10 (Gomez *et al.*, 2013). XRD analysis indicated that the transformation of molybdate-adsorbed ferrihydrite was limited at initial pH 6.5 and 5.0 (Schoepfer *et al.*, 2021).

Effect of sulfide. Reduced sulfur species, particularly sulfide (S(−II)), are key natural reductants that could profoundly alter ferrihydrite transformation pathways and the associated contaminant fate in anoxic environments. Sulfidation, the reaction between Fe(III) oxides and S(−II), leads to reductive iron

dissolution, and the generated Fe(II) may potentially catalyze ferrihydrite transformation into crystalline Fe(III) oxides, which is S(−II) concentration-dependent. At low S(−II)/Fe molar ratios (*e.g.*, < 0.5), sulfidation primarily catalyzed the recrystallization of ferrihydrite into more crystalline Fe(III) oxides, such as goethite and lepidocrocite, especially under slightly acidic conditions (*e.g.*, pH 6) (Wang *et al.*, 2023). At high S(−II)/Fe ratios (*e.g.*, > 0.5), due to the dominance of reductive dissolution, sulfidation mainly leads to the precipitation of Fe(II)-sulfide minerals like mackinawite (FeS) and pyrite (FeS_2), while residual Fe may reprecipitate as secondary Fe(III) oxides (Hockmann *et al.*, 2020; Wang *et al.*, 2023). Therefore, S(-II) does not merely dissolve ferrihydrite but redirects its transformation into distinct Fe minerals (*i.e.*, Fe(III) oxides or Fe(II) sulfides) based on sulfide concentration, while simultaneously immobilizing or transforming the speciation of co-associated contaminants (*e.g.*, arsenic and antimony) (Zhang *et al.*, 2019b; Hockmann *et al.*, 2020). This interplay makes ferrihydrite sulfidation a critical process in controlling iron and trace element cycling in sulfidic soils and sediments.

Effect of organic matter and ligands

In nature, Fe(III) oxides such as ferrihydrite are always associated with NOM or ligands (*e.g.*, FA, HA, and citrate, *etc.*), in the form of mineral-organic aggregates *via* adsorption and/or coprecipitation (Chen and Sparks, 2018; ThomasArrigo *et al.*, 2018; Giannetta *et al.*, 2020). In particular, NOM could be adsorbed on ferrihydrite through electrostatic interactions, hydrogen bonding, ligand exchange, and hydrophobic interactions, which would influence the reactivity of sorbed Fe(II) on ferrihydrite (Huang *et al.*, 2021; Kleber *et al.*, 2021; Dong *et al.*, 2023). OM and organic ligands inhibited Fe(II)-catalyzed conversion of ferrihydrite to more stable Fe minerals, and the extent/degree of inhibition and mechanism depend on the type, concentration/content, and property of OM/ligands (Jones *et al.*, 2009; Chen *et al.*, 2015; ThomasArrigo *et al.*, 2018, 2019; Liu *et al.*, 2025).

Effect of different functional groups of organic matter. The physicochemical properties (*e.g.*, carboxyl content) of coexisting OM play a key roles affecting Fe(II)-induced transformation of ferrihydrite (Zhou *et al.*, 2018; ThomasArrigo *et al.*, 2019; Ding *et al.*, 2025). Organic ligands inhibited Fe(II)-catalyzed ferrihydrite transformations and the formation of crystalline secondary mineral phases compared to pure ferrihydrite. For carboxyl-rich coprecipitates (ferrihydrite-polygalacturonic acid and ferrihydrite-citric acid), mineral transformations were less inhibited than in the carboxyl-poor ferrihydrite-galacturonic acid, and a crystalline lepidocrocite "shell" was formed surrounding the residual ferrihydrite core (ThomasArrigo *et al.*, 2019). Similarly, DOM impeded the formation of goethite and stimulated the formation of lepidocrocite, while only goethite was formed in the presence of polygalacturonic acid (Chen & Sparks, 2018).

In addition, ferrihydrite coprecipitated with HA transformed primarily to goethite after reaction with Fe(II). In contrast, ferrihydrite coprecipitated with FA resulted in no measurable formation of secondary minerals when Fe(II) was present (Zhou *et al.*, 2018). Ferrihydrite formed in the presence of FA or FA-enriched OM was more resistant to transformation than ferrihydrite formed in the presence of humic-like OM, likely due to differences in (i) the amount of surface Fe(II) sorption, (ii) OM molecular weights (MW), or (iii) the carboxylic content of OM. Fulvic acids have higher carboxylic contents compared to HA. It was thus suggested that the carboxylic groups can bind strongly to ferrihydrite surfaces *via* ligand exchange, or associate with Fe(II) (Zhou *et al.*, 2018). Recently, it was also indicated that compared with the low MW OM fraction, the higher MW OM fractions inhibited ferrihydrite transformation less (Liu *et al.*, 2025).

Effect of organic ligand and organic matter amounts/concentrations. The concentrations of organic ligands (*e.g.*, citrate) also significantly affect the types and relative proportions of secondary mineral phases produced during Fe(II)-catalyzed ferrihydrite transformation. As the concentration of citrate gradually increased, the ferrihydrite transformation rate decreased, the relative proportion of goethite in the products decreased, and the relative proportion of lepidocrocite gradually increased (Sheng *et al.*, 2020a).

The carbon (C) content of ferrihydrite-OM coprecipitates strongly impacts the extents and pathways of ferrihydrite transformations and iron atom exchange during its reactions with aqueous Fe(II) (Chen *et al.*, 2015; Chen & Sparks, 2018; Noor & Thompson, 2022). At low C:Fe molar ratios (0–0.05), rapid oxidation of surface-adsorbed ^{57}Fe(II) resulted in ^{57}Fe-enriched crystalline iron minerals and nearly complete mineral transformation within a few days. With increasing OM contents, atom

exchange between aqueous ^{57}Fe(II) and Fe in the organic-rich solids still occurred; however, Fe(II)-catalyzed transformation of ferrihydrite to crystalline minerals was strongly inhibited. For high OM-content materials (C:Fe ≥1.2), Mössbauer spectroscopy revealed up to 39% lepidocrocite in the final Fe(II)-reacted samples (ThomasArrigo *et al.*, 2018).

Roles of natural organic matter: The potential functions. NOM generally suppresses Fe(II)-catalyzed transformation of ferrihydrite to more stable minerals (Jones *et al.*, 2009). Ferrihydrite coprecipitated with NOM (NOM-ferrihydrite) did not transform despite undergoing extensive atom exchange with aqueous Fe(II) (Zhou *et al.*, 2018, 2021). Different roles of OM on Fe(II)-catalyzed ferrihydrite transformation have been proposed (Fig. 2): (i) interfacial electron transfer between sorbed Fe(II) and ferrihydrite or Fe atom exchange on ferrihydrite surfaces is decreased due to surface-site blockage and/or preferential Fe(II) complexation by OM, *i.e.*, formation of Fe(II)-OM solution complexes (Jones *et al.*, 2009; Chen *et al.*, 2018; ThomasArrigo *et al.*, 2017; Chi *et al.*, 2024). OM may reduce the number of potential reaction sites since increased concentrations of OM led to the decrease of the product's surface area, porosity and interparticle interactions as a result of surface coating, clogging of interparticle pores and formation of larger aggregates by OM (Chen *et al.*, 2015); (ii) OM-induced changes to the surface charge of ferrihydrite and the consequent inhibition of growth of more stable mineral phases by suppressing Ostwald ripening and/or oriented aggregation of nuclei (ThomasArrigo *et al.*, 2018; Xiao *et al.*, 2018; Zhou *et al.*, 2018, 2021); (iii) templated growth associated with carboxyl-rich surfaces (ThomasArrigo *et al.*, 2019). The free carboxyl groups in the ferrihydrite-OM coprecipitates could template the growth of crystalline minerals *via* Fe(II) oxidation and hydrolysis (Chan *et al.*, 2004; ThomasArrigo *et al.*, 2019); and (iv) OM can complex and sequester the labile Fe(III) intermediate and thereby disrupt polymerization into stable product minerals (product crystallites) (Sheng *et al.*, 2020a). OM (*e.g.*, citrate) could modify the relative rates of olation (the formation of a μ_2-hydroxide bridge, Fe–OH–Fe) and oxolation (the formation of a μ_2-oxo bridge, Fe–O–Fe) reactions that assembled labile Fe(III) into different iron minerals (Sheng *et al.*, 2020a).

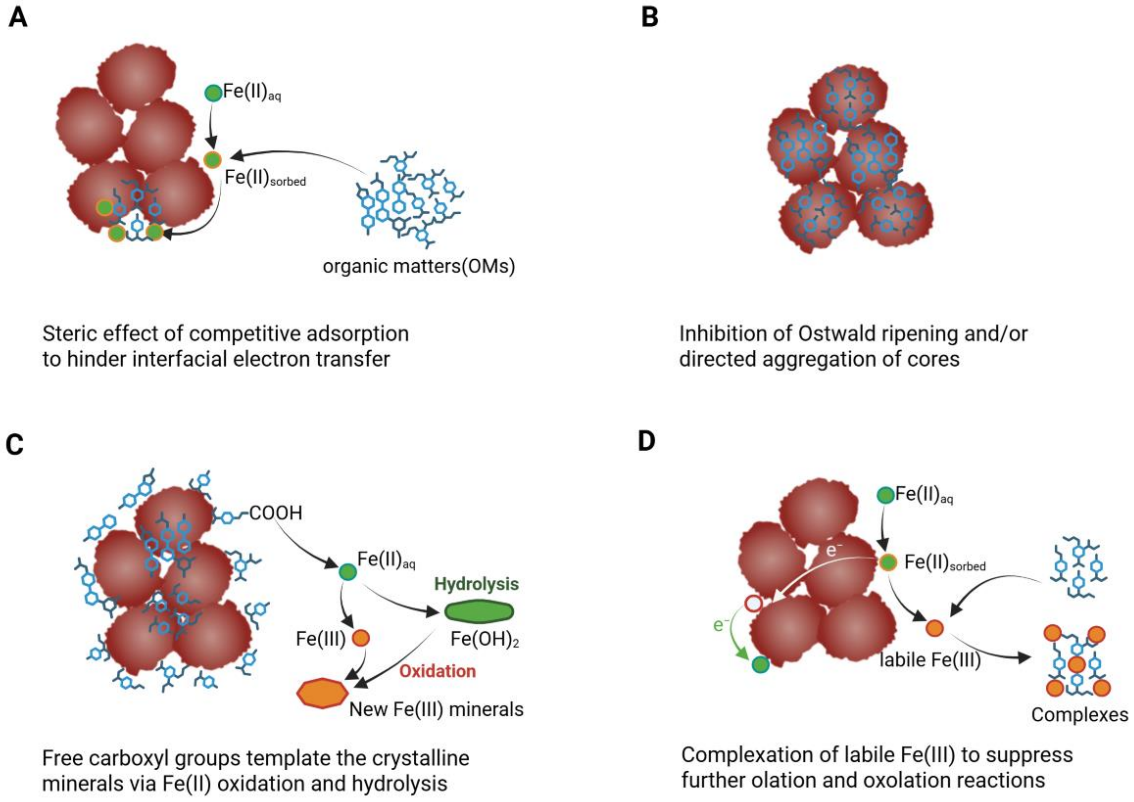

Fig. 2 The proposed mechanisms of organic matter (OM) inhibition effect on Fe(II)-catalyzed ferrihydrite transformation: (A) interfacial electron transfer between sorbed Fe(II) and ferrihydrite or Fe atom exchange at ferrihydrite surfaces is inhibited in the presence of OM; (B) OM-induced changes to the surface charge of

ferrihydrite (toward more negative) and the consequent growth inhibition of more stable mineral phases by suppressing Ostwald ripening and/or oriented aggregation of nuclei; (C) templated growth associated with carboxyl-rich surfaces. The free carboxyl groups in the ferrihydrite-OM coprecipitates could template the growth of crystalline Fe minerals *via* Fe(II) oxidation and hydrolysis; and (D) OM enables the complexation and sequestration of labile Fe(III) intermediates and thereby disrupts polymerization into crystalline Fe(III) oxide minerals (Chen *et al.*, 2015, 2018; ThomasArrigo *et al.*, 2018; Zhou *et al.*, 2018, 2021; Sheng *et al.*, 2020a; Chi *et al.*, 2024).

In turn, changes of Fe mineral composition and properties during the transformation may thus affect the reactivity of Fe(III) oxides toward DOM complexation, as well as the sequestration, transfer, and fate of carbon in soils and sediments (Ding *et al.*, 2022a; Song *et al.*, 2022; Liu *et al.*, 2025). These associated processes could influence global carbon cycling and climate change (Kappler *et al.*, 2021; Dong *et al.*, 2023).

Effect of coexisting minerals

Coexisting solid phases/minerals are another important factor that changes Fe(II)-catalyzed transformation of ferrihydrite in natural environments. Coexisting solid phases/minerals could function as templates for heterogeneous nucleation and growth (Notini *et al.*, 2022), affect electron exchange between ferrihydrite and Fe(II) (Liu *et al.*, 2024), or affect the production and recrystallization of labile Fe(III) by dispersing ferrihydrite aggregates (Wei *et al.*, 2025). For example, it was demonstrated that the addition of goethite (here functioning as nucleation sites) led to more ferrihydrite transformation into goethite during Fe(II)-catalyzed transformation of ferrihydrite (Notini *et al.*, 2022). It was thus hypothesized that electron transfer was promoted *via* a network of conductive goethite-ferrihydrite bands, leading to overall more goethite formation (Notini *et al.*, 2022).

REPARTITIONING OF METAL(LOID)S DURING FERRIHYDRITE TRANSFORMATION

Repartitioning of metal(loid)s during ferrihydrite transformation in the absence of Fe(II)

Ferrihydrite transformation also affects the sequestration, release, and environmental fate of its associated metal(loid)s (*e.g.*, coprecipitates of ferrihydrite and contaminants, and contaminants sorbed on ferrihydrite). Specifically, it has been reported that heavy metals (*e.g.*, Co(II), Zn(II), Pb(II), and Cd(II)) could be incorporated into the crystal structures of transformation products during the transformation of ferrihydrite (Lu *et al.*, 2019, 2020; Sakakibara *et al.*, 2019; Qiu *et al.*, 2023). For example, the concentration of Co(II) greatly affected the structural and magnetic properties of ferrihydrite transformation products. At low cobalt concentrations, cobalt-substituted hematite was formed, while high Co(II) concentrations promoted the formation of cobalt-substituted magnetite (Camacho *et al.*, 2017). Similarly, the initial concentration of Zn(II) affects the redistribution of Zn(II) during ferrihydrite aging transformation. Zinc-bearing maghemite and hematite contained Zn with ~0.4 and ~0.07 of Zn/Fe mole ratios, respectively (Sakakibara *et al.*, 2019). Furthermore, Pb(II) was incorporated into the newly formed hematite, being distributed along the zone axis and enlarging the lattice distance of hematite (Lu *et al.*, 2019, 2020).

EXAFS results have revealed that coexisting anions (*e.g.*, arsenate, selenite, molybdate, vanadate (VO_4^{3-}), and antimonate) could be incorporated or occluded into the structure of ferrihydrite-transformed products (*e.g.*, goethite and hematite) (Mitsunobu *et al.*, 2013; Brinza *et al.*, 2015; Das *et al.*, 2015, 2016; Börsig *et al.*, 2017). It was reported that approximately 1.9wt% of arsenate was incorporated into the structure of newly formed hematite during ferrihydrite transformation, *via* forming short-range ordered clusters similar to those in angelellite ($Fe_4As_2O_{11}$)-like clusters (Bolanz *et al.*, 2013). The extent of arsenate incorporation into hematite increased with the aging time of ferrihydrite-As(V) and ferrihydrite-As(V)-HA coprecipitates at elevated temperature (75 °C) and high pH (~10), as confirmed by Fe and As XAS analyses (Hu *et al.*, 2018). Similarly, selenite could be immobilized within the crystalline products, either by structural incorporation into the hematite lattice (Börsig *et al.*, 2017) or *via* occlusion within nanopores or defect structures (Francisco *et al.*, 2018). Besides these common anions, this incorporation mechanism can extend to radioactive contaminants. Some studies showed

that elements such as Am(III) and U(VI) could also be incorporated into the structure of secondary minerals like goethite and hematite during ferrihydrite transformation (Stumpf *et al.*, 2006; Marshall *et al.*, 2014).

Repartitioning of metal(loid)s during Fe(II)-catalyzed ferrihydrite transformation

Cations and anions (metal micronutrients and contaminants; trace metals and metalloids) associated with ferrihydrite *via* adsorption and coprecipitation could be redistributed during Fe(II)-catalyzed ferrihydrite transformation into secondary minerals, which could change their speciation, mobility, toxicity, and fate in natural environments (Zhang *et al.*, 2019a; Yu *et al.*, 2020). The physicochemical properties of cations (*e.g.*, metal ions) and anions play critical roles in affecting their environmental behavior and fates during Fe(II)-induced recrystallization of ferrihydrite (Liu *et al.*, 2019). Both cations and anions (*e.g.*, metals and metalloids) could be structurally incorporated into or adsorbed onto secondary Fe minerals or form new poorly soluble phases, which may also alter the properties of the secondary Fe minerals (Zhou *et al.*, 2021).

Repartitioning of heavy metals. The repartition of cations (*e.g.*, Cd(II), Cr(III), Zn(II), and Ni(II)) during Fe(II)-catalyzed transformation of ferrihydrite is dependent on cations' physicochemical properties, coexisting OM, concentration of Fe(II), aging time, temperature, and pH (Hu *et al.*, 2022; Yan *et al.*, 2022).

During Fe(II)-catalyzed transformation of ferrihydrite, newly formed secondary minerals may immobilize cations through surface adsorption/complexation, structural substitution/incorporation, surface/bulk precipitation, and physical encapsulation/isolation (physical occlusion), as shown in Fig. 3 (Hu *et al.*, 2019, 2022; Yan *et al.*, 2022; Zhao *et al.*, 2022a). A variety of advanced analytical techniques, such as XAS and spherical aberration corrected scanning transmission electron microscopy (Cs-STEM), are powerful tools and employed to reveal the repartitioning mechanism of heavy metal in atomic scale. For example, during Fe(II)-catalyzed transformation of ferrihydrite with FA-C/Fe molar ratio of 0.21, Cd(II) was dominantly adsorbed on the newly formed lepidocrocite and goethite surfaces in the form of monodentate complexes, as indicated by XAS and energy dispersive X-ray spectroscopy (Hu *et al.*, 2022). The operationally extractable fraction is also widely used to determine the elemental re-distribution during ferrihydrite transformation (Hu *et al.*, 2019; Zhao *et al.*, 2022a). For instance, a positive correlation between the quantity of non-extractable Cd(II) with sodium lactate ($C_3H_5O_3Na$) and magnetite indicated that Cd(II) was incorporated into the lattice structure of newly formed magnetite (Hu *et al.*, 2022).

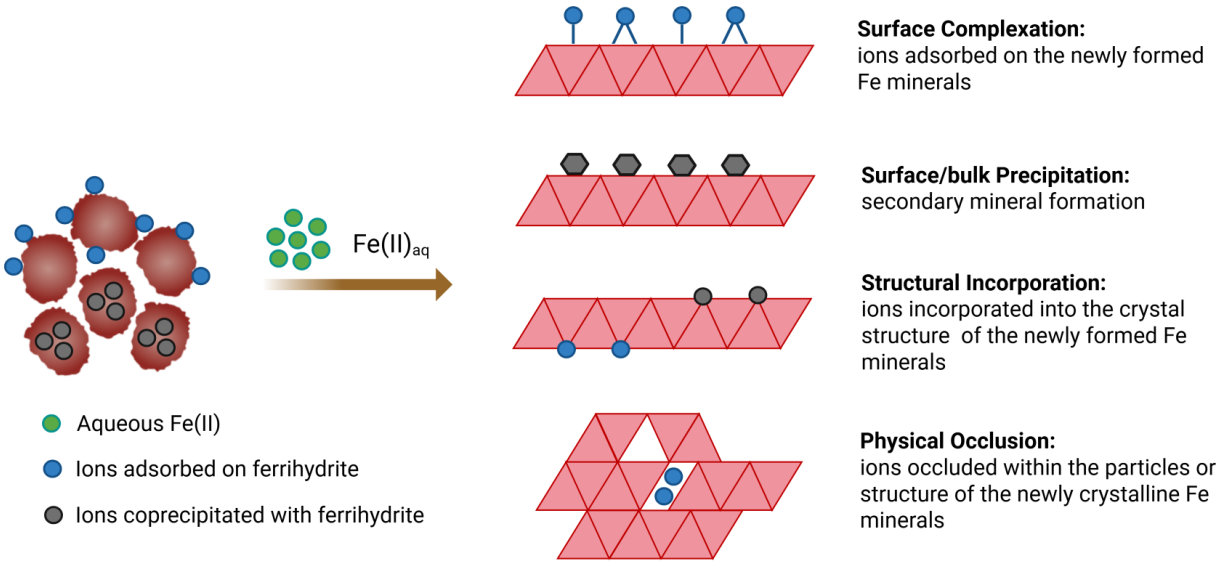

Fig. 3 During Fe(II)-catalyzed ferrihydrite transformation, newly formed secondary minerals may immobilize co-present cations/anions (*e.g.*, Cd(II), Cr(III), As(V), and Se(IV)) through surface complexation, surface/bulk

precipitation, structural incorporation, or physical occlusion (Hu *et al.*, 2019, 2022; Shen *et al.*, 2022; Yan *et al.*, 2022; Zhao *et al.*, 2022a).

External OM (*e.g.*, HA, NOM, and low-molecular-weight carboxyl-rich organic carbon) affected the speciation and partitioning of cations during Fe(II)-catalyzed transformation of ferrihydrite. For instance, compared to Cr(III)-containing ferrihydrite, the presence of OM counteracted the enhancement of Cr(III) extractability during transformation of Cr(III)-containing organo-ferrihydrite coprecipitates. Cs-STEM and XAS analysis suggested that Cr(III) could be incorporated into the newly formed goethite, while its incorporation was inhibited by OM (Xia *et al.*, 2023).

In addition, the presence of OM can also reduce the stabilization of cations during Fe(II)-catalyzed transformation of ferrihydrite (Zhou *et al.*, 2021; Zhao *et al.*, 2023b). In the presence of Fe(II), Ni associated with NOM-ferrihydrite (ferrihydrite coprecipitated with NOM and Ni) was more susceptible to 0.1 M HCl extraction than ferrihydrite (ferrihydrite coprecipitated with Ni), suggesting that NOM limited Ni incorporation into secondary Fe minerals and reduced Ni stabilization (Zhou *et al.*, 2021).

During Fe(II)-catalyzed ferrihydrite transformation, U(VI) was also reduced to a U(V) species, which finally incorporated into goethite and magnetite (Nico *et al.*, 2009; Boland *et al.*, 2014a). Structural impurities of ferrihydrite (*e.g.*, Si and Al) could greatly affect the speciation and repartitioning of hexavalent uranium (U(VI)) during Fe(II)-catalyzed transformation (Boland *et al.*, 2011; Massey *et al.*, 2014). For instance, during Fe(II)-catalyzed transformation, the extent of U(V) incorporation into goethite (the product of transformed Al-ferrihydrite), decreased substantially (from 70 to 30%) with increasing Al contents (from 0 to 20%). The decrease in U incorporation with increasing Al contents was due to two main factors: (i) decreased transformation of ferrihydrite to goethite; and (ii) alternation of the goethite lattice with increasing Al contents, making the lattice less compatible with large U atoms (Massey *et al.*, 2014).

Oxidation or reduction of anions/oxyanions. During Fe(II)-catalyzed transformation of ferrihydrite, the redox status of coexisting anions/oxyanions may be altered (*i.e.*, be oxidized or reduced), depending on the reaction condition (Perez *et al.*, 2019; Zhang *et al.*, 2019a). For instance, during Fe(II)-catalyzed transformation of ferrihydrite, As(III) could be oxidized to As(V) and As(V) could be reduced to As(III). A considerable fraction of As(III) (70–80%) was oxidized to As(V) during the transformation of As(III)-adsorbed ferrihydrite (Zhang *et al.*, 2019a).

In addition, it was reported that a small fraction of Se(IV) was reduced to elemental Se during this process, as indicated by the XANES results (Wang *et al.*, 2020). Moreover, antimony (Sb) K-edge XANES spectroscopy analysis demonstrated a significant reduction of up to 60% reduction of solid-phase Sb(V) to Sb(III) during Fe(II)-induced transformation of Sb(V)-ferrihydrite (Karimian *et al.*, 2019).

Release and sequestration of anions/oxyanions. Fe(II)-catalyzed transformation of ferrihydrite also affects the mobilization or immobilization of anions/oxyanions. The extractable proportion of these anions/oxyanions, determined through wet chemistry analysis (*e.g.*, using phosphate or NaOH solution to extract anions/oxyanions in the reaction products), can be used to assess their binding/associating strength to minerals (*e.g.*, being incorporated and/or occluded, or forming new minerals), as shown in Fig. 3 (Hockmann *et al.*, 2021; Zhao *et al.*, 2022b; Wang *et al.*, 2025).

For example, during the recrystallization of ferrihydrite, 1 M phosphate-extractable As decreased quickly by up to 90% in the solid phase, indicating that partial As transformed to a stable phase (Zhang *et al.*, 2019a). The portions of 0.1 M NaOH non-extractable As increased with aging time in ferrihydrite-As and ferrihydrite-As-FA (C/Fe = 0.25 and 0.42) treatments, and the amount of non-extractable As(V) was positively correlated with the amount of formed crystalline Fe(III) oxides during the ferrihydrite transformation processes, indicating that As sequestration was strongly associated with the newly formed lepidocrocite and goethite (Hu *et al.*, 2020). Approximately 30–75% of the adsorbed Se(IV) transformed into a phosphate-unextractable form, indicating that Se(IV) was incorporated and/or occluded within the particles of crystalline goethite or formed other poorly soluble Se-bearing phases during the transformation of ferrihydrite (Wang *et al.*, 2020). These findings underscore that anion sequestration is closely tied to mineral recrystallization, with reduced extractability reflecting structural occlusion or stable phase formation.

Mechanistic studies indicate that anions/oxyanions could be incorporated into the structure of the newly formed iron oxides during ferrihydrite transformation (Hu *et al.*, 2020; Schoepfer *et al.*, 2020,

2021; Wang *et al.*, 2025). For instance, during Fe(II)-induced transformation of ferrihydrite-As(V)-FA coprecipitates, besides surface adsorption (on defective surface sites or into the nano pore spaces), a portion of As(V) may be incorporated into the lattice structures of newly formed crystalline Fe(III) oxides (*i.e.*, goethite and lepidocrocite), as indicated by EXAFS analysis (Hu *et al.*, 2020). The Sb K-edge EXAFS results showed that Sb(V) immobilization was due to incorporation of Sb(V) into Fe(III) octahedral sites of the newly formed secondary minerals (*e.g.*, goethite) *via* heterovalent substitution for Fe(III) (Hockmann *et al.*, 2021).

These mechanisms highlight that anion retention during ferrihydrite transformation is not only limited to surface interactions but also involves dynamic structural reorganization, including surface complexation (*i.e.*, re-adsorption onto newly formed Fe minerals), secondary mineral precipitation, structural incorporation, and physical occlusion. The dominance of a specific mechanism depends on the chemical nature of these anions (*e.g.*, charge, ionic radius, and coordination chemistry), the presence of competing species (*e.g.*, OM), and the transformation pathway (*i.e.*, the identity and crystallinity of the product minerals). Consequently, the transition of the anions from an "exchangeable" to a "non-extractable" state represents a kinetic and thermodynamic outcome of coupled Fe mineral phase transformation and anion-mineral interface evolution. Our mechanistic framework provides a critical foundation for predicting and managing the long-term stability and environmental risk of oxyanion contaminants in iron-rich anaerobic environments (Fig. 3).

CONCLUSIONS

This review summarizes the key processes and mechanisms involved in the transformation of ferrihydrite, with a special focus on Fe(II)-catalyzed transformation. Ferrihydrite transforms into more thermodynamically stable and crystalline iron oxides (*e.g.*, goethite, lepidocrocite, magnetite, and hematite) with the rate and extent regulated by a variety of environmental factors (*e.g.*, temperature, pH, and the presence of other substances). Under Fe(II)-free conditions, ferrihydrite slowly transforms to goethite or hematite either through a dissolution-recrystallization process (with goethite being an intermediary) or through a solid state-phase transformation. Meanwhile, in the presence of Fe(II), ferrihydrite easily transforms to crystalline Fe(III) oxides *via* Fe(II)-catalyzed dissolution-reprecipitation and solid-state transformation. In this case, labile Fe(III) species play a key role in these transformation processes. In Fe(II)-free systems, coexisting ions, OM, and solid substances could enhance ferrihydrite transformation by promoting the aggregation and modulating the dissolution-recrystallization process, and inhibit ferrihydrite transformation by retarding the hydrolysis and dissolution of ferrihydrite, reducing the aggregation, or complexing with aqueous Fe(III) to inhibit the nucleation. Surface-associated or coprecipitated anions/cations, ligands, OM, or coexisting other substances affect the rates and extent of Fe(II)-catalyzed ferrihydrite transformation, as well as the transformation pathways, the identity, and the crystalline structures of the products. The coexisting anions/cations/ligands/OM usually inhibit Fe(II)-catalyzed ferrihydrite transformation by blocking the electron transfer between Fe(II) and structural Fe(III), suppressing labile Fe(III) generation, and hindering the dissolution, polymerization, and recrystallization of Fe(III). The transformation of ferrihydrite holds potential environmental, mineralogical, and geological implications, such as regulation of the speciation and bioavailability of nutrient elements, sequestration of OM, immobilization of pollutants, and remediation of contaminated environments (Wang *et al.*, 2020; Yan *et al.*, 2022; Zhao *et al.*, 2022b). The associated trace anions/cations are redistributed into secondary iron oxide minerals during the transformation of ferrihydrite, *via* surface complexation, surface/bulk precipitation, structural incorporation, and physical occlusion.

Although significant progress has been made in understanding ferrihydrite transformation and its Fe(II)-catalyzed pathways, the reaction processes and molecular-level mechanisms under complex environmental conditions still need to be further explored. Building on current knowledge, future research should prioritize the following areas:

i) State-of-the-art techniques, including in-situ spectroscopic techniques, spatially resolved techniques, and microscope techniques, could be applied to elucidate the transformation process (Liu *et al.*, 2022b), particularly with respect to interfacial electron transfer and pore confinement. With the help of advanced characterization techniques (*e.g.*, confocal micro-Raman spectroscopy and HR-TEM) with sufficient temporal resolution at micrometer or nanometer level (Grigg et al., 2022), more studies

are needed to further reveal the structure and the growth processes of the secondary mineral particles during ferrihydrite transformation in the presence or absence of Fe(II) (Sheng *et al.*, 2020b). Quasi in-situ identical location transmission electron microscopy (IL-TEM) could be used to visualize ferrihydrite transformation and secondary mineral particles distribution at the atomic scale (Sheng *et al.*, 2021) and provide visual evidence and quantitation of both ferrihydrite dissolution and product phase growth rates.

ii) Elucidate the reaction mechanism over a longer timescale. It is necessary to investigate the speciation and environmental behavior (*e.g.*, mobility, redistribution/partitioning, and fate) of nutrients, OM, and pollutants during the transformation of ferrihydrite over a long period of time, such as several months or years, which depends on ferrihydrite residence time in different environmental matrices.

iii) The effect of fluctuating redox conditions. In real environments, *e.g.*, floodplains (anoxic zones), riverine wetland zones (redox alternating zones), riverbank zones (oxic zones), riparian zones, and flooded paddy soils (anoxic environments), fluctuating redox reactions triggered by oxygen fluctuations commonly occur (Zhao *et al.*, 2023a; Schulz *et al.*, 2024). For example, freshwater wetlands often undergo frequent and rapid changes in the redox potential resulting from fluctuating water tables and shifts in microbial activity. Therefore, the effect of fluctuating redox conditions on the transformation of ferrihydrite should be considered.

iv) Quasi-real environment. The rates and pathways of ferrihydrite transformation processes have been studied intensely in model systems or ideal conditions, but the transformation of ferrihydrite in a quasi-real environment is not well studied and understood (Grigg *et al*., 2022; Lefebvre *et al*., 2024; ThomasArrigo *et al*., 2024). It was reported that Fe(II)-catalyzed ferrihydrite transformation experiments in soils and sediments were quite different from abiotic model studies in laboratory systems (Notini *et al.*, 2023). More microcosmic experiments (*e.g.*, incubation experiments with added ^{57}Fe-labeled ferrihydrite or aqueous Fe(II)) of soils and sediments should be performed in future research to track the ferrihydrite formation and transformation in natural environments.

DECLARATION OF COMPETING INTEREST

The authors declare that they have no known competing financial interests or personal relationships that could have appeared to influence the work reported in this paper.

ACKNOWLEDGMENTS

This research is supported by the National Natural Science Foundation of China (Grant Nos. 42167031 and 42407326) and Distinguished Young Scholars of the National Natural Science Foundation of China (Overseas) (B.W.), the Natural Science Foundation of Jiangxi (Grant No. 20242BAB25198), and the Fundamental Research Funds for the Central Universities-Huazhong Agricultural University (B.W.). M.M. acknowledges the support of the DFG (Project ID 494840258) and Foreign Expert Program of the Ministry of Human Resources and Social Security of P.R.C. (Grant No. H20250389). All schematic figures were created in Biorender.com.

REFERENCES

Amstaetter K, Borch T, Larese-Casanova P, Kappler A. 2010. Redox transformation of arsenic by Fe(II)-activated goethite (α-FeOOH). *Environ Sci Technol*. **44**: 102–108.

Arinchtein A, Schmack R, Kraffert K, Radnik J, Dietrich P, Sachse R, Kraehnert R. 2020. Role of water in phase transformations and crystallization of ferrihydrite and hematite. *ACS Appl Mater Interfaces*. **12**: 38714–38722.

Berquó T S, Banerjee S K, Ford R G, Penn R L, Pichler T. 2007. High crystallinity Si-ferrihydrite: An insight into its Néel temperature and size dependence of magnetic properties. J Geophys Res Solid Earth. **112**: B2.

Boland D D, Collins R N, Glover C J, Payne T E, Waite T D. 2014a. Reduction of U(VI) by Fe(II) during the Fe(II)-Accelerated Transformation of Ferrihydrite. *Environ Sci Technol*. **48**: 9086–9093.

Boland D D, Collins R N, Glover C J, Waite T D. 2013. An *in situ* quick-EXAFS and redox potential

study of the Fe(II)-catalysed transformation of ferrihydrite. *Colloids Surf A Physicochm Eng Asp*. **435**: 2–8.

Boland D D, Collins R N, Miller C J, Glover C J, Waite T D. 2014b. Effect of solution and solid-phase conditions on the Fe(II)-accelerated transformation of ferrihydrite to lepidocrocite and goethite. *Environ Sci Technol*. **48**: 5477–5485.

Boland D D, Collins R N, Payne T E, Waite T D. 2011. Effect of amorphous Fe(III) oxide transformation on the Fe(II)-mediated reduction of U(VI). *Environ Sci Technol*. **45**: 1327−1333.

Bolanz R M, Wierzbicka-Wieczorek M, Čaplovičová M, Uhlík P, Göttlicher J, Steininger R, Majzlan J. 2013. Structural incorporation of As^{5+} into hematite. *Environ Sci Technol*. **47**: 9140−9147.

Börsig N, Scheinost AC, Shaw S, Schild D, Neumann T. 2017. Uptake mechanisms of selenium oxyanions during the ferrihydrite-hematite recrystallization. *Geochim Cosmochim Acta*. **206**: 236–253.

Brinza L, Vu H P, Shaw S, Fred J, Mosselmans W, Benning L G. 2015. Effect of Mo and V on the hydrothermal crystallization of hematite from ferrihydrite: An *in situ* energy dispersive X-ray diffraction and X-ray absorption spectroscopy study. *Cryst Growth Des*. **15**: 4768–4780.

Camacho K I, Pariona N, Martinez A I, Baggio-Saitovitch E, Herrera-Trejo M, Perry D L. 2017. Structural and magnetic properties of the products of the transformation of ferrihydrite: Effect of cobalt dications. *J Magn Magn Mater*. **429**: 339–347.

Chan C S, De S G, Welch S A, Girasole M, Frazer B H, Nesterova M V, Fakra S, Banfield J F. 2004. Microbial polysaccharides template assembly of nanocrystal fibers. *Science*. **303**: 1656−1658.

Chappell H F, Thom W, Bowron D T, Faria N, Hasnip P J, Powell J J. 2017. Structure of naturally hydrated ferrihydrite revealed through neutron diffraction and first-principles modeling. *Phys Rev Mater*. **1**: 036002.

Chen A, Li Y, Shang J, Arai Y. 2020. Ferrihydrite transformation impacted by coprecipitation of phytic acid. *Environ Sci Technol*. **54**: 8837–8847.

Chen C, Kukkadapu R, Sparks D L. 2015. Influence of coprecipitated organic matter on $Fe^{2+}_{(aq)}$-catalyzed transformation of ferrihydrite: Implications for carbon dynamics. *Environ Sci Technol*. **49**: 10927–10936.

Chen C, Sparks D L. 2018. Fe(II)-induced mineral transformation of ferrihydrite–organic matter adsorption and co-precipitation complexes in the absence and presence of As(III). *ACS Earth Space Chem*. **2**: 1095–1101.

Cheng L, Ding Y, Liu Y, Chen J, Wu X, Liu J, Wang L, Sheng A. 2025. Pore-size-dependent kinetics and product distribution of Fe(II)-catalyzed ferrihydrite transformation. *Environ Sci Technol.* **59**: 12667–12678.

Chi J, Ou Y, Li F, Zhang W, Zhai H, Liu T, Chen Q, Zhou X, Fang L. 2024. Cooperative roles of phosphate and dissolved organic matter in inhibiting ferrihydrite transformation and their distinct fates. *Sci Total Environ*. **908**: 168376.

Cornell R M, Schwertmann U. 2003. The Iron Oxides: Structure, Properties, Reactions, Occurrences and Uses, Wiley-VCH, Weinheim, Germany.

Cudennec Y, Lecerf A. 2006. The transformation of ferrihydrite into goethite or hematite, revisited. J *Solid State Chem*. **179**: 716–722.

Das S, Essilfie-Dughan J, Hendry M J. 2015. Fate of adsorbed arsenate during phase transformation of ferrihydrite in the presence of gypsum and alkaline conditions. *Chem Geol*. **411**: 69–80.

Das S, Essilfie-Dughan J, Hendry M J. 2016. Sequestration of molybdate during transformation of 2-line ferrihydrite under alkaline conditions. *App Geochem*. **73**: 70–80.

Das S, Hendry M J, Essilfie-Dughan J. 2011a. Effects of adsorbed arsenate on the rate of transformation of 2-Line ferrihydrite at pH 10. *Environ Sci Technol*. **45**: 5557–5563.

Das S, Hendry M J, Essilfie-Dughan J. 2011b. Transformation of two-Line ferrihydrite to goethite and hematite as a function of pH and temperature. *Environ Sci Technol*. **45**: 268–275.

Ding L, Han B, Jia R, Yang X, Liang X, Guo X. 2025. Molecular insights into the synergistic inhibition of microplastics-derived dissolved organic matter and anions on the transformation of ferrihydrite. *Environ Sci Technol*. **59**: 4104–4112.

Ding Y, Huang X, Zhang H, Ma J, Li F, Zeng Q, Hu N, Wang Y, Dai Z, Ding D. 2022a. Coupled variations of dissolved organic matter distribution and iron (oxyhydr)oxides transformation: Effects on the kinetics of uranium adsorption and desorption. *J Hazard Mater*. **435**: 129298.

Ding Y, Sheng A, Li X, Liu Y, Yan M, Takahashi Y, Liu J. 2024. Triplet-excited riboflavin promotes labile Fe(III) accumulation and changes mineralization pathways in Fe(II)-catalyzed ferrihydrite transformation. *Environ Sci Technol*. **58**: 22148–22158.

Ding Z, Sun G, Fu F, Ye C. 2022b. Phase transformation of Cr(VI)-adsorbed ferrihydrite in the presence of Mn(II): Fate of Mn(II) and Cr(VI). *J Environ Sci*. **113**: 251–259.

Dong Y, Wang J, Ma C, Thompson A, Liu C, Chen C. 2024. The influence of seawater on Fe(II)-catalyzed ferrihydrite transformation and its subsequent consequences for C dynamics. *Environ Sci Technol*. **58**: 19277–19288.

Dong H, Zeng Q, Sheng Y, Chen C, Yu G, Kappler A. 2023. Coupled iron cycling and organic matter transformation across redox interfaces. *Nat Rev Earth Environ*. **4**: 659–673.

Drits VA, Sakharov BA, Salyn AL, Manceau A. 1993. Structural model for ferrihydrite. *Clay Miner*. **28**: 185–207.

Fei Y, Hua J, Liu C, Li F, Zhu Z, Xiao T, Chen M, Gao T, Wei Z, Hao L. 2018. Aqueous Fe(II)-induced phase transformation of ferrihydrite coupled adsorption/immobilization of rare earth elements. *Minerals*. **8**: 357.

Ford R G. 2002. Rates of hydrous ferric oxide crystallization and the influence on coprecipitated arsenate. *Environ Sci Technol*. **36**: 2459−2463.

Francisco P C M, Sato T, Otake T, Kasama T, Suzuki S, Shiwaku H, Yaita T. 2018. Mechanisms of Se(IV) co-precipitation with ferrihydrite at acidic and alkaline conditions and its behavior during aging. *Environ Sci Technol.* **52**: 4817−4826.

Funnell N P, Fulford M F, Inoué S, Kletetschka K, Michel F M, Goodwin A L. 2020. Nanocomposite structure of two-line ferrihydrite powder from total scattering. *Commun Chem*. **3**: 22.

Furcas F E, Lothenbach B, Mundra S, Borca C N, Albert C C, Isgor O B, Huthwelker T, Angst U M. 2023. Transformation of 2-line ferrihydrite to goethite at alkaline pH. *Environ Sci Technol*. **57**: 16097–16108.

Giannetta B, Balint R, Said-Pullicino D, Plaza C, Martin M, Zaccone C. 2020. Fe(II)-catalyzed transformation of Fe (oxyhydr) oxides across organic matter fractions in organically amended soils. *Sci Total Environ*. **748**: 141125.

Gilbert B, Erbs J J, Penn R L, Petkov V, Spagnoli D, Waychunas G A. 2013. A disordered nanoparticle model for 6-line ferrihydrite. *Am Mineral*. **98**: 1465–1476.

Gomez M A, Hendry M J, Hossain A, Das S, Elouatik S. 2013. Abiotic reduction of 2-line ferrihydrite: effects on adsorbed arsenate, molybdate, and nickel. *RSC Adv*. **3**: 25812−25822.

Gomez M A, Jiang R, Song M, Li D, Lea A S, Ma X, Wang H, Yin X, Wang S, Jia Y. 2020. Further insights into the Fe(II) reduction of 2-line ferrihydrite: A semi *in situ* and *in situ* TEM study. *Nanoscale Adv*. **2**: 4938−4950.

Grigg A R C, ThomasArrigo L K, Schulz K, Rothwell K A, Kaegi R, Kretzschmar R. 2022. Ferrihydrite transformations in flooded paddy soils: rates, pathways, and product spatial distributions. *Environ Sci Proc Imp*. **24**: 1867–1882.

Handler R M, Beard B L, Johnson C M, Scherer M M. 2009. Atom exchange between aqueous Fe(II) and goethite: An Fe isotope tracer study. *Environ Sci Technol*. **43**: 1102–1107.

Hansel C M, Benner S G, Fendorf S. 2005. Competing Fe(II)-induced mineralization pathways of ferrihydrite. *Environ Sci Technol*. **39**: 7147–7153.

Hansel C M, Learman D R, Lentini C J, Ekstrom E B. 2011. Effect of adsorbed and substituted Al on Fe(II)-induced mineralization pathways of ferrihydrite. *Geochim Cosmochim Acta*. **75**: 4653–4666.

Harrington R, Hausner D B, Xu W, Bhandari N, Michel F M, Brown G E, Strongin D R, Parise J B. 2011. Neutron pair distribution function study of two-line ferrihydrite. *Environ Sci Technol*. **45**: 9883–9890.

Hiemstra T. 2013. Surface and mineral structure of ferrihydrite. *Geochim Cosmochim Acta*. **105**: 316–325.

Hiemstra T. 2015. Formation, stability, and solubility of metal oxide nanoparticles: Surface entropy, enthalpy, and free energy of ferrihydrite. *Geochim Cosmochim Acta*. **158**: 179–198.

Hinkle M A G, Catalano J G. 2015. Effect of phosphate and sulfate on Ni repartitioning during Fe(II)-catalyzed Fe(III) oxide mineral recrystallization. *Geochim Cosmochim Acta*. **165**: 62–74.

Hockmann K, Karimian N, Schlagenhauff S, Planer-Friedrich B, Burton E D. 2021. Impact of antimony(V) on iron(II)-catalyzed ferrihydrite transformation pathways: A novel mineral switch

for feroxyhyte formation. *Environ Sci Technol*. **55**: 4954–4963.
Hockmann K, Planer-Friedrich B, Johnston S G, Peiffer S, Burton E D. 2020. Antimony mobility in sulfidic systems: Coupling with sulfide-induced iron oxide transformations. *Geochim Cosmochim Acta*. **282**: 276–296.
Hu S, Liang Y, Liu T, Li F, Lu Y, Shi Z. 2020. Kinetics of As(V) and carbon sequestration during Fe(II)-induced transformation of ferrihydrite-As(V)-fulvic acid coprecipitates. *Geochim Cosmochim Acta*. **272**: 160–176.
Hu S, Lu Y, Peng L, Wang P, Zhu M, Dohnalkova A C, Chen H, Lin Z, Dang Z, Shi Z. 2018. Coupled kinetics of ferrihydrite transformation and As(V) sequestration under the effect of humic acids: A mechanistic and quantitative study. *Environ Sci Technol*. **52**: 11632–11641.
Hu S, Zhen L, Liu S, Liu C, Shi Z, Li F, Liu T. 2022. Synchronous sequestration of cadmium and fulvic acid by secondary minerals from Fe(II)-catalyzed ferrihydrite transformation. *Geochim Cosmochim Acta*. **334**: 83–98.
Hu Y, Xue Q, Tang J, Fan X, Chen H H. 2019. New insights on Cr(VI) retention by ferrihydrite in the presence of Fe(II). *Chemosphere*. **222**: 511–516.
Hua J, Liu C, Li F, Zhu Z, Wei Z, Chen M, Gao T, Qiu G. 2019. Effects of rare earth elements' physicochemical properties on their stabilization during the $Fe(II)_{aq}$-induced phase transformation of ferrihydrite. *ACS Earth Space Chem*. **3**: 895–904.
Hua J, Sun J, Chen M, Liu C, Wu F. 2023. Aqueous Fe(II)-catalyzed iron oxide recrystallization Fe redox cycling and atom exchange, mineralogical recrystallization and contributing factor. *Rev Environ Sci Bio*. **22**: 55–78.
Huang J, Jones A, Waite T D, Chen Y, Huang X, Rosso K M, Kappler A, Mansor M, Tratnyek P G, Zhang, H. 2021. Fe(II) redox chemistry in the environment. *Chem Rev*. **121**: 8161–8233.
Janney D E, Cowley J M, Buseck P R. 2000. Structure of synthetic 2-line ferrihydrite by electron nanodiffraction. *Am Miner*. **85**: 1180–1187.
Jones A M, Collins R N, Rose J, Waite T D. 2009. The effect of silica and natural organic matter on the Fe(II)-catalysed transformation and reactivity of Fe(III) minerals. *Geochim Cosmochim Acta*. **73**: 4409–4422.
Jones A M, Collins R N, Waite T D. 2017. Redox characterization of the Fe(II)-catalyzed transformation of ferrihydrite to goethite. *Geochim Cosmochim Acta*. **218**: 257–272.
Kappler A, Bryce C, Mansor M, Lueder U, Byrne J M, Swanner E D. 2021. An evolving view on biogeochemical cycling of iron. *Nat Rev Microbiol*. **19**: 360–374.
Karimian N, Burton E D, Johnston S G, Hockmann K, Choppala G. 2019. Humic acid impacts antimony partitioning and speciation during iron(II)-induced ferrihydrite transformation. *Sci Total Environ*. **683**: 399−410.
Kleber M, Bourg I, Coward E, Hansel C, Myneni S, Nunan N. 2021. Dynamic interactions at the mineral-organic matter interface. *Nat Rev Earth Environ*. **2**: 402–421.
Latta D, Rosso K M, Scherer M M. 2023. Tracking initial Fe(II)-driven ferrihydrite transformations: A Mössbauer spectroscopy and isotope investigation. *ACS Earth Space Chem.* **7**: 1814–1824.
Lefebvre P, Grigg A R C, Kretzschmar R. 2024. Geochemical decoupling of iron and zinc during transformation of Zn-bearing ferrihydrite in reducing sediments. *Environ Sci Technol.* **58**: 20224–20234.
Li Y, Yang M, Pentrak M, He H, Arai Y. 2020. Carbonate-enhanced transformation of ferrihydrite to hematite. *Environ Sci Technol*. **54**: 13701–13708.
Li Y, Zhang C, Yang M, He H, Arai Y. 2022. Carbonate accelerated transformation of ferrihydrite in the presence of phosphate. *Geoderma*. **417**: 115811.
Lin Z, Fu F, Yu G, Sun G, Tang B. 2022. Fate of Cr(VI) during aging of ferrihydrite-humic acid co-precipitates: Comparative studies of structurally incorporated Al(III) and Mn(II). *Sci Total Environ*. **807**: 151073.
Liu C, Chen M, Li F, Tao L, Lin J, Gao T, Tong H, Liu Y, Long S, Wu F, Xia Y. 2019. Stabilization of Cd^{2+}/Cr^{3+} during aqueous Fe(II)-induced recrystallization of Al-substituted goethite. *Soil Sci Soc Am J*. **83**: 483–491.
Liu C, Li F, Chen M, Liao C, Tong H, Hua J. 2017. Adsorption and stabilization of lead during Fe(II)-catalyzed phase transformation of ferrihydrite. *Acta Chim Sinica.* **75**: 621–628.
Liu C, Zhu Z, Li F, Liu T, Liao C, Lee J J, Shih K, Tao L, Wu Y. 2016. Fe(II)-induced phase

transformation of ferrihydrite: The inhibition effects and stabilization of divalent metal cations. *Chem Geol*. **444**: 110–119.
Liu F, Liang Y, Zhu R, Xiao J, Xing J, Zhu L, Ye Q, Lv Y, Shi Z. 2025. Probing molecular level and subnanoscale stabilization mechanisms of organic carbon species during Fe(II)-induced ferrihydrite transformation. *Environ Sci Technol*. **59**: 13832–13843.
Liu H, Guo H, Li P, Wei Y. 2008. The transformation of ferrihydrite in the presence of trace Fe(II): The effect of the anionic media. *J Solid State Chem*. **181**: 2666–2671.
Liu H, Li P, Zhu M, Wei Y, Sun Y. 2007. Fe(II)-induced transformation from ferrihydrite to lepidocrocite and goethite. *J Solid State Chem*. **180**: 2121–2128.
Liu H, Ma M, Qin M, Yang L, Wei Y. 2010a. Studies on the controllable transformation of ferrihydrite. *J Solid State Chem*. **183**: 2045–2050.
Liu H, Wei Y, Sun Y H. 2005. The Formation of hematite from ferrihydrite using Fe(II) as a catalyst. *J Mol Catal A Chem*. **226**: 135–140.
Liu H, Yang L J, Ma M R, Li P, Wei Y. 2010b. The transformation of ferrihydrite in the presence of trace Fe(II): The effect of the ammonia, amine and the coordination ions of Fe(III). *J Solid State Chem*. **183**: 542–546.
Liu J, Chen Q, Yang Y, Wei H, Laipan M, Zhu R, He H, Hochella M F. 2022a. Coupled redox cycling of Fe and Mn in the environment: The complex interplay of solution species with Fe-and Mn-(oxyhydr)oxide crystallization and transformation. *Earth-Sci Rev*. **232**: 104105.
Liu J, Sheng A, Li X, Arai Y, Ding Y, Nie M, Yan M, Rosso K M. 2022b. Understanding the importance of labile Fe(III) during Fe(II)-catalyzed transformation of metastable iron oxyhydroxides. *Environ Sci Technol*. **56**: 3801–3811.
Liu N, Zhang Y, Chen M, Lei Q, Dong L, Tong H, Liu C, Yu H. 2024. Influence of biochar on the $Fe(II)_{aq}$-catalyzed transformation of ferrihydrite. *ACS Earth Space Chem*. **8**: 2027–2037.
Liu Y, Ding Y, Sheng A, Li X, Chen J, Arai Y, Liu J. 2023. Fe(II)-catalyzed transformation of ferrihydrite with different degrees of crystallinity. *Environ Sci Technol*. **57**: 6934–6943.
Lu Y, Hu S, Liang Z, Zhu M, Wang Z, Wang Z, Liang W, Dang Z, Shi Z. 2020. Incorporation of Pb(II) into hematite during ferrihydrite transformation. *Environ Sci Nano*. **7**: 829–841.
Lu Y, Hu S, Wang Z, Ding Y, Lu G, Lin Z, Dang Z, Shi Z. 2019. Ferrihydrite transformation under the impact of humic acid and Pb: kinetics, nanoscale mechanisms, and implications for C and Pb dynamics. *Environ Sci Nano*. **6**: 747–762.
Lv Y, Liu J, Zhu R, Zhu J, Chen Q, Liang X, He H. 2022. Photoreductive dissolution of iron (hydr)oxides and its geochemical significance. *ACS Earth Space Chem*. **6**: 811–829.
Manceau A. 2009. Evaluation of the structural model for ferrihydrite derived from real-space modelling of high-energy X-ray diffraction data. *Clay Miner*. **44**: 19–34.
Manceau A, Skanthakumar S, Soderholm L. 2014. PDF analysis of ferrihydrite: Critical assessment of the under-constrained akdalaite model. *Am Miner*. **99**: 102–108.
Marchand P, Rancourt D G. 2009. General model for the aqueous precipitation of rough-surface nanocrystals and application to ferrihydrite genesis. *Am Miner*. **94**: 1428–1439.
Marshall T A, Morris K, Law G T W, Livens F R, Mosselmans J F W, Bots P, Shaw S. 2014. Incorporation of Uranium into Hematite during Crystallization from Ferrihydrite. *Environ Sci Technol*. **48**: 3724–3731.
Massey M S, Lezama-Pacheco J S, Michel F M, Fendorf S. 2014. Uranium incorporation into aluminum-substituted ferrihydrite during iron(II)-induced transformation. *Environ Sci Proc Imp*. **16**: 2137–2144.
Masue-Slowey Y, Loeppert RH, Fendorf S. 2011. Alteration of ferrihydrite reductive dissolution and transformation by adsorbed As and structural Al: Implications for As retention. *Geochim Cosmochim Acta*. **75**: 870–886.
Michel F M, Barrón V, Torrent J, Morales M P, Serna C J, Boily J F, Liu Q, Ambrosini A, Cismasu A C, Brown G E. 2010. Ordered ferrimagnetic form of ferrihydrite reveals links among structure, composition and magnetism. *Procs Nat Acad Sci*. **107**: 2787–2792.
Michel F M, Ehm L, Antao S M, Lee P L, Chupas P J, Liu G, Strongin D R, Schoonen M A A, Phillips B L, Parise J B. 2007. The structure of ferrihydrite, a nanocrystalline material. *Science*. **316**: 1726−1729.
Mitsunobu S, Muramatsu C, Watanabe K, Sakata M. 2013. Behavior of antimony(V) during the

transformation of ferrihydrite and its environmental implications. *Environ Sci Technol*. **47**: 9660–9667.

Namayandeh A, Borkiewicz O J, Bompoti N M, Chrysochoou M, Michel F M. 2022. Oxyanion surface complexes control the kinetics and pathway of ferrihydrite transformation to goethite and hematite. *Environ Sci Technol*. **56**: 15672–15684.

Namayandeh A, Borkiewicz O J, Bompoti N M, Watson S K, Kubicki J D, Chrysochoou M, Michel F M. 2023. Effects of oxyanion surface loading on the rate and pathway of ferrihydrite transformation. *ACS Earth Space Chem*. **7**: 2154–2165.

Namayandeh A, Zhang W, Watson S K, Borkiewicz O J, Bompoti N M, Chrysochoou M, Lee Penn R, Michel F M. 2024. Goethite and hematite nucleation and growth from ferrihydrite: Effects of oxyanion surface complexes. *Environ Sci Technol*. **58**: 5952–5962.

Navrotsky A, Mazeina L, Majzlan J. 2008. Size-driven structural and thermodynamic complexity in iron oxides. *Science*. **319**: 1635–1638.

Nico P S, Stewart B D, Fendorf S. 2009. Incorporation of oxidized uranium into Fe (hydr)oxides during Fe(II) catalyzed remineralization. *Environ Sci Technol*. **43**: 7391–7396.

Noor N, Thompson A. 2022. Localized alteration of ferrihydrite natural organic matter coprecipitates following reaction with Fe(II). *Soil Sci Soc Am J*. **86**: 253–263.

Notini L, Schulz K, Kubeneck L J, Grigg A R C, Rothwell K A, Fantappiè G, ThomasArrigo L K, Kretzschmar R. 2023. A new approach for investigating iron mineral transformations in soils and sediments using ^{57}Fe-labeled minerals and ^{57}Fe Mössbauer spectroscopy. *Environ Sci Technol.* **57**: 10008−10018.

Notini L, ThomasArrigo L K, Kaegi R, Kretzschmar R. 2022. Coexisting goethite promotes Fe(II)-catalyzed transformation of ferrihydrite to goethite. *Environ Sci Technol*. **56**: 12723–12733.

Pan X, Huang X, Deng N. 2025. Short-chain carboxylic acids influencing mineralization mechanisms of ferrihydrite transformation to hematite and goethite. *Environ Sci Technol.* **59**: 12910−12919.

Peak D, Regier T. 2012. Direct observation of tetrahedrally coordinated Fe(III) in ferrihydrite. *Environ Sci Technol*. **46**: 3163–3168.

Pedersen H D, Postma D, Jakobsen R, Larsen O. 2005. Fast transformation of iron oxyhydroxides by the catalytic action of aqueous Fe(II). *Geochim Cosmochim Acta*. **69**: 3967−3977.

Pedersen H D, Postma D, Jakobsen R. 2006. Release of arsenic associated with the reduction and transformation of iron oxides. *Geochim Cosmochim Acta*. **70**: 4116−4129.

Perez J P H, Tobler D J, Thomas A N, Freeman H M, Dideriksen K, Radnik J, Benning L G. 2019. Adsorption and reduction of arsenate during the Fe^{2+}-induced transformation of ferrihydrite. *ACS Earth Space Chem*. **3**: 884–894.

Pinney N, Kubicki J D, Middlemiss D S, Grey C P, Morgan D. 2009. Density functional theory study of ferrihydrite and related fe-oxyhydroxides. *Chem Mater*. **21**: 5727–5742.

Qafoku O, Kovarik L, Bowden M E, Nakouzi E. Sheng A, Liu J, Pearce C I, Rosso K M. 2020. Nanoscale observations of Fe(II)-induced ferrihydrite transformation. *Environ Sci Nano*. **7**: 2953-2967.

Qiu J, Hou X, Ren Y, Liu C, Meng F, Lee J F, Lin Y J, Huang Z, Ma H, Shi Z, Feng C. 2023. Photoinduced transformation of ferrihydrite in the presence of aqueous sulfite and its influence on the repartitioning of Cd. *Water Res*. **231**: 119607.

Sakakibara M, Tanaka M, Takahashi Y, Murakami T. 2019. Redistribution of Zn during transformation of ferrihydrite: Effects of initial Zn concentration. *Chem Geol*. **522**: 121–134.

Sassi M, Chaka A M, Rosso K M. 2021. Ab initio thermodynamics reveals the nanocomposite structure of ferrihydrite. *Commun Chem*. **4**: 134.

Sassi M, Rosso K M. 2022. Ab initio evaluation of solid-state transformation pathways from ferrihydrite to goethite. *ACS Earth Space Chem*. **6**: 800–809.

Schoepfer V A, Lum J E, Lindsay M B J. 2021. Molybdenum(VI) Sequestration Mechanisms During Iron(II)-Induced Ferrihydrite Transformation. *ACS Earth Space Chem*. **5**: 2094–2104.

Schoepfer V A, Qin K X, Robertson J M, Das S, Lindsay M B J. 2020. Structural incorporation of sorbed molybdate during iron(II)-induced transformation of ferrihydrite and goethite under advective flow conditions. *ACS Earth Space Chem*. **4**: 1114–1126.

Schulz K, Notini L, Grigg A R C, Kubeneck L J, Wisawapipat W, ThomasArrigo L K, Kretzschmar R. 2023. Contact with soil impacts ferrihydrite and lepidocrocite transformations during redox

cycling in a paddy soil. *Environ Sci Proc Imp.* **25**: 1945−1961.
Schulz K, ThomasArrigo L K, Kaegi R, Kretzschmar R. 2022. Stabilization of ferrihydrite and lepidocrocite by silicate during Fe(II)-catalyzed mineral transformation: Impact on particle morphology and silicate distribution. *Environ Sci Technol*. **56**: 5929–5938.
Schulz K, Wisawapipat W, Barmettler K, Grigg A R C, Kubeneck L J, Notini L, ThomasArrigo L K, Kretzschmar R. 2024. Iron oxyhydroxide transformation in a flooded rice paddy field and the effect of adsorbed phosphate. *Environ Sci Technol.* **58**: 10601–10610.
Schwertmann U, Friedl J, Kyek A. 2004. Formation and properties of a continuous crystallinity series of synthetic ferrihydrites (2-to 6-line) and their relation to FeOOH forms. *Clays Clay Miner*. **52**: 221–226.
Schwertmann U, Murad E. 1983. Effect of pH on the formation of goethite and hematite from ferrihydrite. *Clays Clay Miner*. **31**: 277−284.
Schwertmann U, Stanjek H, Becher H H. 2004. Long-term in vitro transformation of 2-line ferrihydrite to goethite/hematite at 4, 10, 15 and 25 °C. *Clay Miner*. **39**: 433−438.
Shen X, Zhu H, Wang P, Zheng L, Hu S, Liu C. 2022. Mechanistic and modeling insights into the immobilization of Cd and organic carbon during abiotic transformation of ferrihydrite induced by Fe(II). *J Hazard Mater*. **436**: 129216.
Sheng A, Li X, Arai Y, Ding Y, Rosso K M, Liu J. 2020a. Citrate controls Fe(II)-catalyzed transformation of ferrihydrite by complexation of the labile Fe(III) intermediate. *Environ Sci Technol*. **54**: 7309–7319.
Sheng A, Liu J, Li X, Qafoku O, Collins R N, Jones A M, Pearce C I, Wang C, Ni J, Lu A, Rosso K M. 2020b. Labile Fe(III) from sorbed Fe(II) oxidation is the key intermediate in Fe(II)-catalyzed ferrihydrite transformation. *Geochim Cosmochim Acta*. **272**: 105–120.
Sheng A, Liu J, Li X, Luo L, Ding Y, Chen C, Zhang X, Wang C, Rosso K M. 2021. Labile Fe(III) supersaturation controls nucleation and properties of product phases from Fe(II)-catalyzed ferrihydrite transformation. *Geochim Cosmochim Acta*. **309**: 272–285.
Shu Z, Liu L, Tan W, Suib S L, Qiu G, Yang X, Zheng L, Liu F. 2019. Solar irradiation induced transformation of ferrihydrite in the presence of aqueous Fe^{2+}. *Environ Sci Technol.* **53**: 8854−8861.
Shu Z, Pan Z, Wang X, He H, Yan S, Zhu X, Song W, Wang Z. 2022. Sunlight-induced interfacial electron transfer of ferrihydrite under oxic conditions: Mineral transformation and redox active species production. *Environ Sci Technol.* **56**: 14188–14197.
Soltis J A, Feinberg J M, Gilbert B, Penn R L. 2016. Phase transformation and particle-mediated growth in the formation of hematite from 2-Line ferrihydrite. *Cryst Growth Des*. **16**: 922–932.
Song X, Wang P, Zwieten L V, Bolan N, Wang H, Li X, Cheng K, Yang Y, Wang M, Liu T, Li F. 2022. Towards a better understanding of the role of Fe cycling in soil for carbon stabilization and degradation. *Carbon Res*. **1**: 5.
Sun G, Fu F, Tang B. 2022. Fate of metal-EDTA complexes during ferrihydrite aging: Interaction of metal-EDTA and iron oxides. *Chemosphere*. **291**: 132791.
Sun G, Fu F, Yu G, Yu P, Tang B. 2021. Migration behavior of Cr(VI) during the transformation of ferrihydrite-Cr(VI) co-precipitates: The interaction between surfactants and co-precipitates. *Sci Total Environ*. **767**: 145429.
Stumpf S, Stumpf T, Dardenne K, Hennig C, Foerstendorf H, Klenze R, Fanghänel T. 2006. Sorption of Am(III) onto 6-line-ferrihydrite and its alteration products: Investigations by EXAFS. *Environ Sci Technol*. **40**: 3522–3528.
ThomasArrigo L K, Byrne J M, Kappler A, Kretzschmar R. 2018. Impact of organic matter on iron(II)-catalyzed mineral transformations in ferrihydrite–organic matter coprecipitates. *Environ Sci Technol*. **52**: 12316-12326.
ThomasArrigo L K, Kaegi R, Kretzschmar R. 2019. Ferrihydrite growth and transformation in the presence of ferrous iron and model organic ligands. *Environ Sci Technol*. **53**: 13636–13647.
ThomasArrigo L K, Mikutta C, Byrne J, Kappler A, Kretzschmar R. 2017. Iron(II)-catalyzed iron atom exchange and mineralogical changes in iron-rich organic freshwater flocs: An iron isotope tracer study. *Environ Sci Technol*. **51**: 6897–6907.
ThomasArrigo L K, Notini L, Vontobel S, Bouchet S, Nydegger T, Kretzschmar R. 2024. Emerging investigator series: Coprecipitation with glucuronic acid limits reductive dissolution and transformation of ferrihydrite in an anoxic soil. *Environ Sci Proc Imp.* **26**: 1489–1502.

Wang C, Ying C, Wang W, Zhou S, Wan B, Tan W, Feng X. 2025. Sunlight-driven transformation of ferrihydrite *via* ligand-to-metal charge transfer: The critical factors and arsenic repartitioning. *Environ Sci Technol*. **59**: 6567−6578.

Wang Q, Wang J, Wang X, Kumar N, Pan Z, Peiffer S, Wang Z. 2023. Transformations of ferrihydrite−extracellular polymeric substance coprecipitates driven by dissolved sulfide: Interrelated effects of carbon and sulfur loadings. *Environ Sci Technol.* **57**: 4342–4353.

Wang S, Lei L, Zhang D, Zhang G, Cao R, Wang X, Lin J, Jia Y. 2020. Stabilization and transformation of selenium during the Fe(II)-induced transformation of Se(IV)-adsorbed ferrihydrite under anaerobic conditions. *J Hazard Mater*. **384**: 121365.

Wang X, Li W, Harrington R, Liu F, Parise J B, Feng X, Sparks D L. 2013. Effect of ferrihydrite crystallite size on phosphate adsorption reactivity. *Environ Sci Technol*. **47**: 10322–10331.

Wang X, Zhu M, Koopal L K, Li W, Xu W, Liu F, Zhang J, Liu Q, Feng X, Sparks D L. 2016. Effects of crystallite size on the structure and magnetism of ferrihydrite. *Environ Sci Nano*. **3**: 190–202.

Wang Z, Xiao D, Bush R T, Liu J. 2015. Coprecipitated arsenate inhibits thermal transformation of 2-line ferrihydrite: Implications for long-term stability of ferrihydrite. *Chemosphere*. **122**: 88–93.

Weatherill J S, Morris K, Bots P, Stawski T M, Janssen A, Abrahamsen L, Blackham R, Shaw S. 2016. Ferrihydrite formation: The role of Fe_{13} Keggin clusters. *Environ Sci Technol*. **50**: 9333–9342.

Wei H, Liu J, Chen Q, Yang Y, Xian H, Liang X, Yang Y, Zhu J, Zhu R. 2025. Coexisting hematite induces and accelerates the transformation of ferrihydrite: Pathway and underlying mechanisms. *Am Miner*. **110**: 430–445.

Wei H, Wei S, Chen Q, Yang Y, Liu X, Long S, Liu J, Zhu J, Zhu R, Scale N. 2025. Insights into clay minerals regulating the Fe(II)-catalyzed ferrihydrite transformation under anoxic conditions. *Environ Sci Technol*. **59**: 3982–3991.

Xia X, Liu J, Jin L, Wang J, Darma A I, He C, Shakouri M, Hu Y, Yang J. 2023. Organic matter counteracts the enhancement of Cr(III) extractability during the Fe(II)-catalyzed ferrihydrite transformation: A nanoscale- and molecular-level investigation. *Environ Sci Technol*. **57**: 13496–13505.

Xiao W, Jones A M, Collins R N, Bligh M W, Waite T D. 2017. Use of Fourier transform infrared spectroscopy to examine the Fe(II)-catalyzed transformation of ferrihydrite. *Talanta*. **175**: 30–37.

Xiao W, Jones A M, Collins R N, Waite T D. 2018. Investigating the effect of ascorbate on the Fe(II)-catalyzed transformation of the poorly crystalline iron mineral ferrihydrite. *Biochim Biophys Acta Gen Subj*. **1862**: 1760–1769.

Yan J, Frierdich A J, Catalano J G. 2022. Impact of Zn substitution on Fe(II)-induced ferrihydrite transformation pathways. *Geochim Cosmochim Acta*. **320**: 143–160.

Yan L, Chen Q, Yang Y, Zhu R. 2021. The significant role of montmorillonite on the formation of hematite nanoparticles from ferrihydrite under heat treatment. *Appl Clay Sci*. **202**: 105962.

Yang L, Steefel C I, Marcus M A, Bargar J R. 2010. Kinetics of Fe(II)-catalyzed transformation of 6-line ferrihydrite under anaerobic flow conditions. *Environ Sci Technol*. **44**: 5469–5475.

Yang M J, Liang X L, Li Y, He H P, Zhu R L, Arai Y J. 2021. Ferrihydrite Transformation impacted by adsorption and structural incorporation of rare earth elements. *ACS Earth Space Chem*. **5**: 2768–2777.

Ye C, Ariya P A, Fu F, Yu G, Tang B. 2021. Influence of Al(III) and Sb(V) on the transformation of ferrihydrite nanoparticles: Interaction among ferrihydrite, coprecipitated Al(III) and Sb(V). *J Hazard Mater*. **408**: 124423.

Yee N, Shaw S, Benning L G, Nguyen T H. 2006. The rate of ferrihydrite transformation to goethite *via* the Fe(II) pathway. *Am Miner*. **91**: 92–96.

Yu G, Fu F, Ye C, Tang B. 2020. Behaviors and fate of adsorbed Cr(VI) during Fe(II)-induced transformation of ferrihydrite-humic acid co-precipitates. *J Hazard Mater*. **392**: 122272.

Zhang D, Wang S, Wang Y, Gomez M A, Duan Y, Jia Y. 2018. The transformation of two-line ferrihydrite into crystalline products: Effect of pH and media (sulfate versus nitrate). *ACS Earth Space Chem*. **2**: 577–587.

Zhang G, Yuan Z, Lei L, Lin J, Wang X, Wang S, Jia Y. 2019a. Arsenic redistribution and transformation during Fe(II)-catalyzed recrystallization of As-adsorbed ferrihydrite under anaerobic conditions. *Chem Geol*. **525**: 380–389.

Zhang G, Zhang D, Yuan Z, Ma X, Lei L, Wu X, Lin J, Wang X, Wang S, Jia J. 2019b. Fate of adsorbed

arsenic during early stage sulfidization of nano-ferrihydrite. *Environ Sci Nano* **6**: 2228–2240.
Zhang M, Ding L, Qiu X, Liang X, Huang Y, Shan X, Chen Q, Guo X. 2024. Interactions between iron minerals and dissolved organic matter derived from microplastics inhibited the ferrihydrite transformation as revealed at the molecular scale. *Environ Sci Technol*. **58**: 13478–13489.
Zhang T, Tang B, Fu F. 2023. Influence of montmorillonite incorporation on ferrihydrite transformation and Cr(VI) behaviors during ferrihydrite-Cr(VI) coprecipitates aging. *Sci Total Environ*. **873**: 162257.
Zhao G, Tan M, Wu B, Zheng X, Xiong R, Chen B, Kappler A, Chu C. 2023a. Redox oscillations activate thermodynamically stable iron minerals for enhanced reactive oxygen species production. *Environ Sci Technol.* **57**: 8628–8637.
Zhao W, Sheng A, Liu Z, Feng X, Tan W, Wang X. 2025. Fe(II)-catalyzed transformation of phosphate-bearing ferrihydrite: Mineralogical mechanisms and phosphate fate. *Environ Sci Technol.* **59**: 25332–25343.
Zhao X, Yuan Z, Wang S, Pan Y, Chen N, Tunc A, Cheung K, Alparov A, Chen W, Deevsalar R, Lin J, Jia Y. 2022a. Iron(II)-activated phase transformation of Cd-bearing ferrihydrite: Implications for cadmium mobility and fate under anaerobic conditions. *Sci Total Environ*. **848**: 157719.
Zhao X, Yuan Z, Wang S, Zhang G, Qu S, Wang Y, Liu S, Pan Y, Lin J, Jia Y. 2022b. The fate of co-existent cadmium and arsenic during Fe(II)-induced transformation of As(V)/Cd(II)-bearing ferrihydrite. *Chemosphere*. **301**: 134665.
Zhao Y, Moore O W, Xiao K Q, Curti L, Otero Fariña A, Banwart S A, Peacock C L. 2022c. The role and fate of organic carbon during aging of ferrihydrite. *Geochim Cosmochim Acta*. **335**: 339–355.
Zhao Y, Moore O W, Xiao K Q, Otero-Fariña A, Banwart S A, Wu F C, Peacock C L. 2023b. Behavior and fate of chromium and carbon during Fe(II)-induced transformation of ferrihydrite organominerals. *Environ Sci Technol*. **57**: 17501–17510.
Zhou Z, Latta D E, Noor N, Thompson A, Borch T, Scherer M M. 2018. Fe(II)-catalyzed transformation of organic matter-ferrihydrite coprecipitates: A closer look using Fe isotopes. *Environ Sci Technol*. **52**: 11142–11150.
Zhou Z, Latta D E, Scherer M M. 2021. Natural organic matter inhibits Ni stabilization during Fe(II)-catalyzed ferrihydrite transformation. *Sci Total Environ*. **755**: 142612.